From:	Jeff Meucci <jrmeucciscuba@gmail.com>
Sent:	Wednesday, May 11, 2022 8:55 AM
To:	Debra Thompson
Subject:	Fwd: SE sea otter survey
Attachments:	Leach et al_2021_Ecology_optimal design in ecological studies.pdf; Lu2022_Article_ImprovingWildlifePopulationInf.pdf; Eisaguirre_et_al_2021_diffusion_model_SE.pdf

Hi Debbie, could you please include this information in this week's packet. Just informational. Thanks

Sent from my iPad

Begin forwarded message:

> **From:** "Schuette, Paul A" <paul_schuette@fws.gov>
> **Date:** May 2, 2022 at 10:40:43 AM AKDT
> **To:** Kathy Hansen <kathy@seafa.org>, "Cate, Jenipher R" <jenipher_cate@fws.gov>, Bo Meredith <bo.meredith@alaska.gov>, "Eisaguirre, Joseph M" <joseph_eisaguirre@fws.gov>, Ginny Eckert <gleckert@alaska.edu>, Jeff Muecci <jrmeucciscuba@gmail.com>, John Moller <jmofish@yahoo.com>, Katy Bear <KNalven@defenders.org>, "Lemons, Patrick R" <Patrick_Lemons@fws.gov>, "Larsen Tempel, Jenell T (DFG)" <jenell.larsentempel@alaska.gov>, Lynn Lee <lynn.lee2@canada.ca>, Mike Jackson <dot@kake-nsn.gov>, Mike Miller <go2tbird@hotmail.com>, Phil Doherty <info@sardfa.org>, Ralph Wolfe <rwolfe2@ccthita-nsn.gov>, Sam Rabung <samuel.rabung@alaska.gov>, ttinker <ttinker@nhydra.com>, "Weitzman, Benjamin P" <benjamin_weitzman@fws.gov>, Kate Sullivan <ksullivan@sardfa.org>, Maya Becker <maya_becker@murkowski.senate.gov>, Carly Besh <carly_besh@murkowski.senate.gov>, "Nichols, Carina (Sullivan)" <Carina_Nichols@sullivan.senate.gov>, "Lee Kadinger (lee.kadinger@sealaska.com)" <lee.kadinger@sealaska.com>, "O'Connor, Jamie (Murkowski)" <Jamie_O'Connor@murkowski.senate.gov>, "Cummings, Caroline E" <caroline_cummings@fws.gov>, Perry J Williams <perryw@unr.edu>, "Lemons, Patrick R" <Patrick_Lemons@fws.gov>
> **Subject: SE sea otter survey**

Hello,

We wanted to provide everyone an update on our sea otter population survey across southeast Alaska. First, we will be working with Owyhee Air Research to conduct aerial, photo-based population surveys starting May 17, 2022. The survey will require two weeks of flight time, but we have allocated our time and resources to be available through June 30, if necessary, to accommodate poor weather.

Over the past two years, we have designed a sea otter population survey and will be analyzing the data with the most up-to-date methods (see attached papers). Given the high interest among stakeholders, we also wanted to give extra consideration to 10 communities. As a result, we have included transects within a 20km (12.4 mile) radius of each of these communities.

We wanted to share with you our survey maps in advance of the survey. Our hope is that you can view, discuss, and circulate these maps and provide us with any comments by May 9. We will do our best to address comments in advance of the start of the survey, working within the resources available to us (e.g. the amount of flight time we have available for the survey).

Second, we are planning to rotate our base of operations for the field team (2-4 FWS biologists) and the Owyhee flight team (pilot, camera operator) across Juneau, Sitka, Petersburg/Wrangell, and Ketchikan based on airstrip and fueling options to maximize efficiency. We will adapt when/where we are based depending on weather conditions. Although we hope to solidify lodging in advance, we anticipate we will sometimes have to make last-minute adjustments. We would welcome any recommendations for local, back-up options for places to stay (or camp) in case we get in a jam. Please feel free to send us any local options that come to mind.

Thank you for your input as this project has developed. We look forward to not only conducting the survey, but hopefully, finding a way to meet up with many of you informally during our time in southeast, if possible. We will do our best to keep you updated on our location as we move around the area.
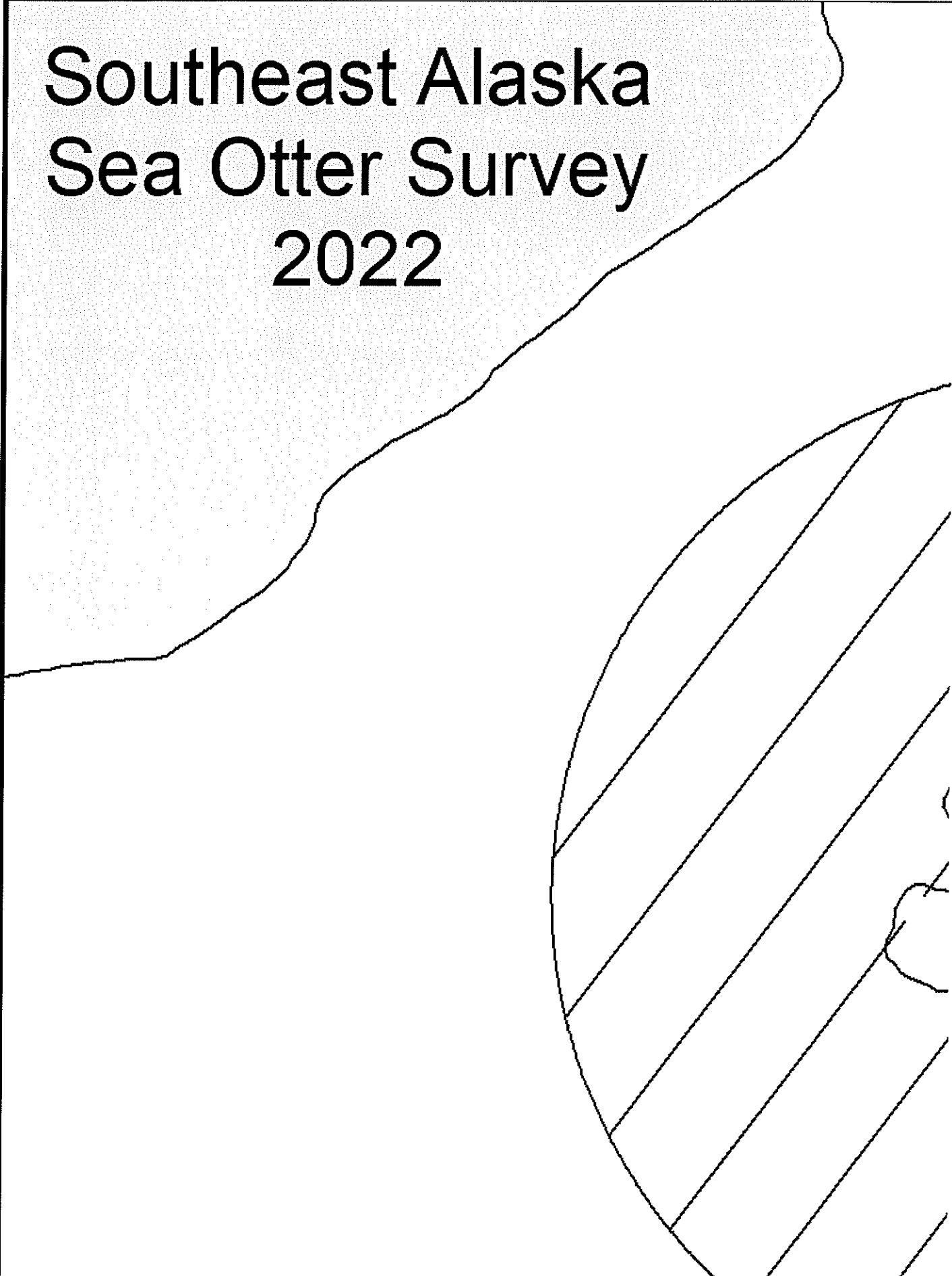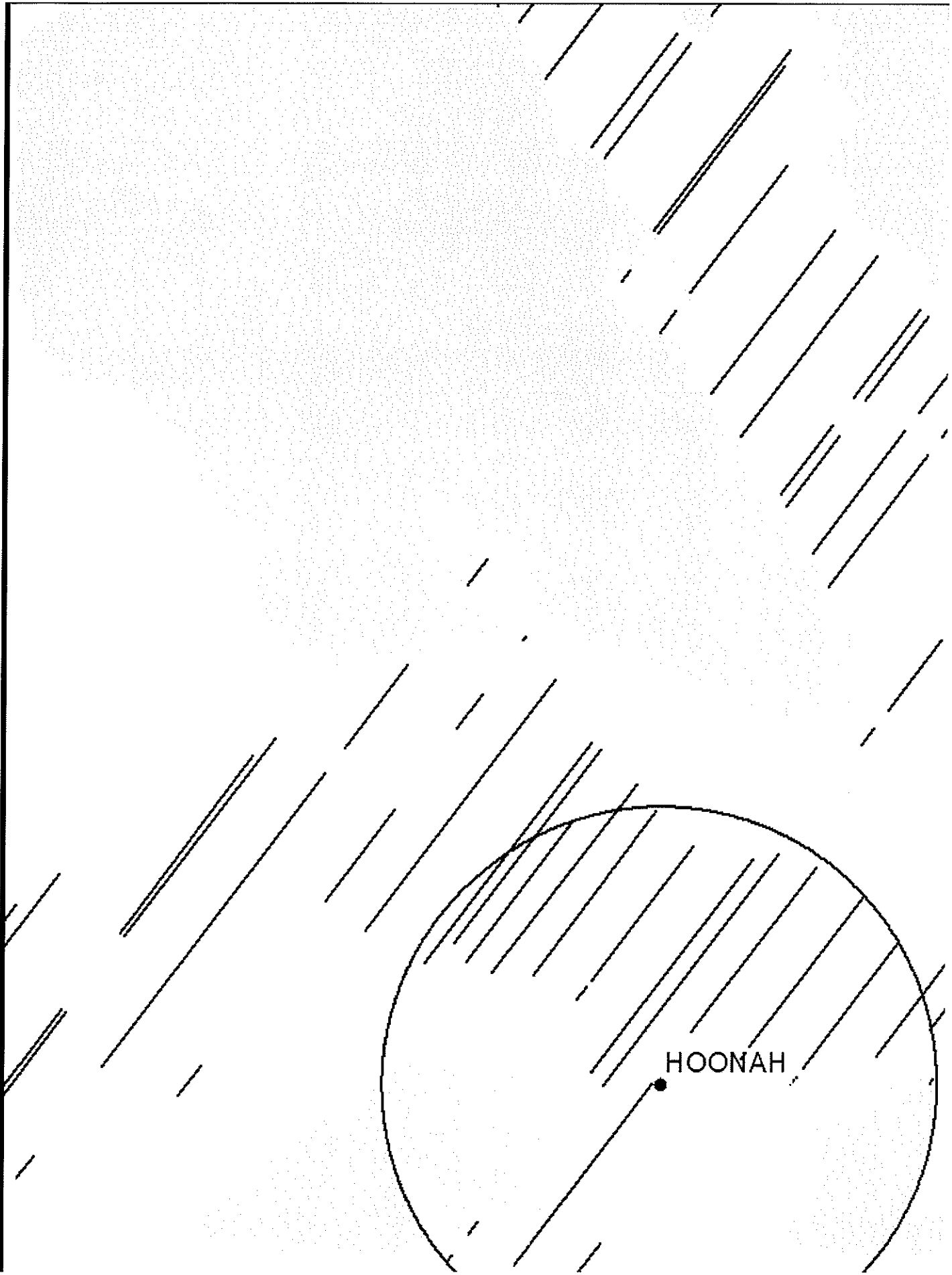
Best,
Paul

Paul Schuette, Ph.D.
Marine Mammals Management
U.S. Fish and Wildlife Service
1011 E. Tudor Rd., MS-341
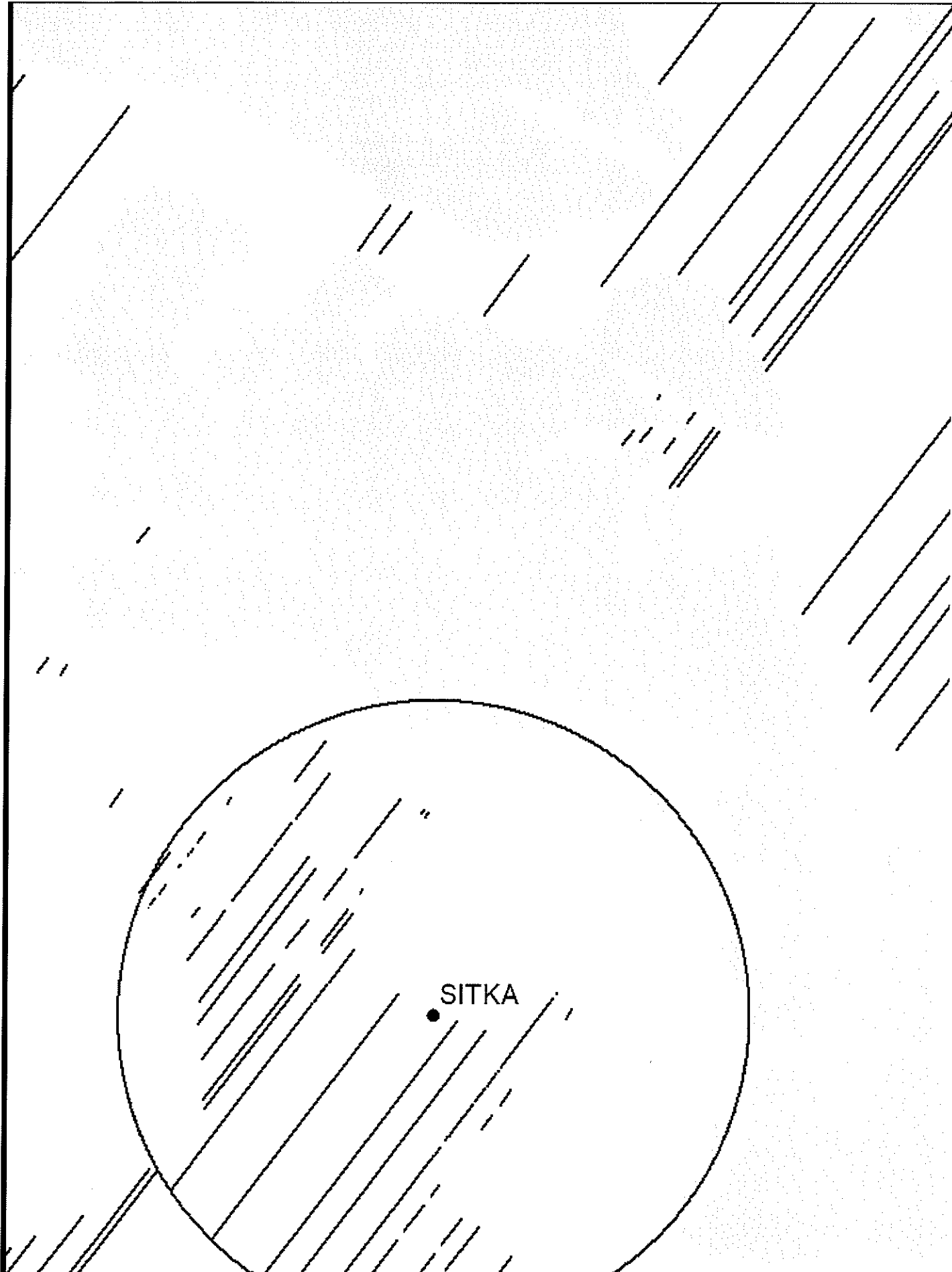Anchorage, AK 99503
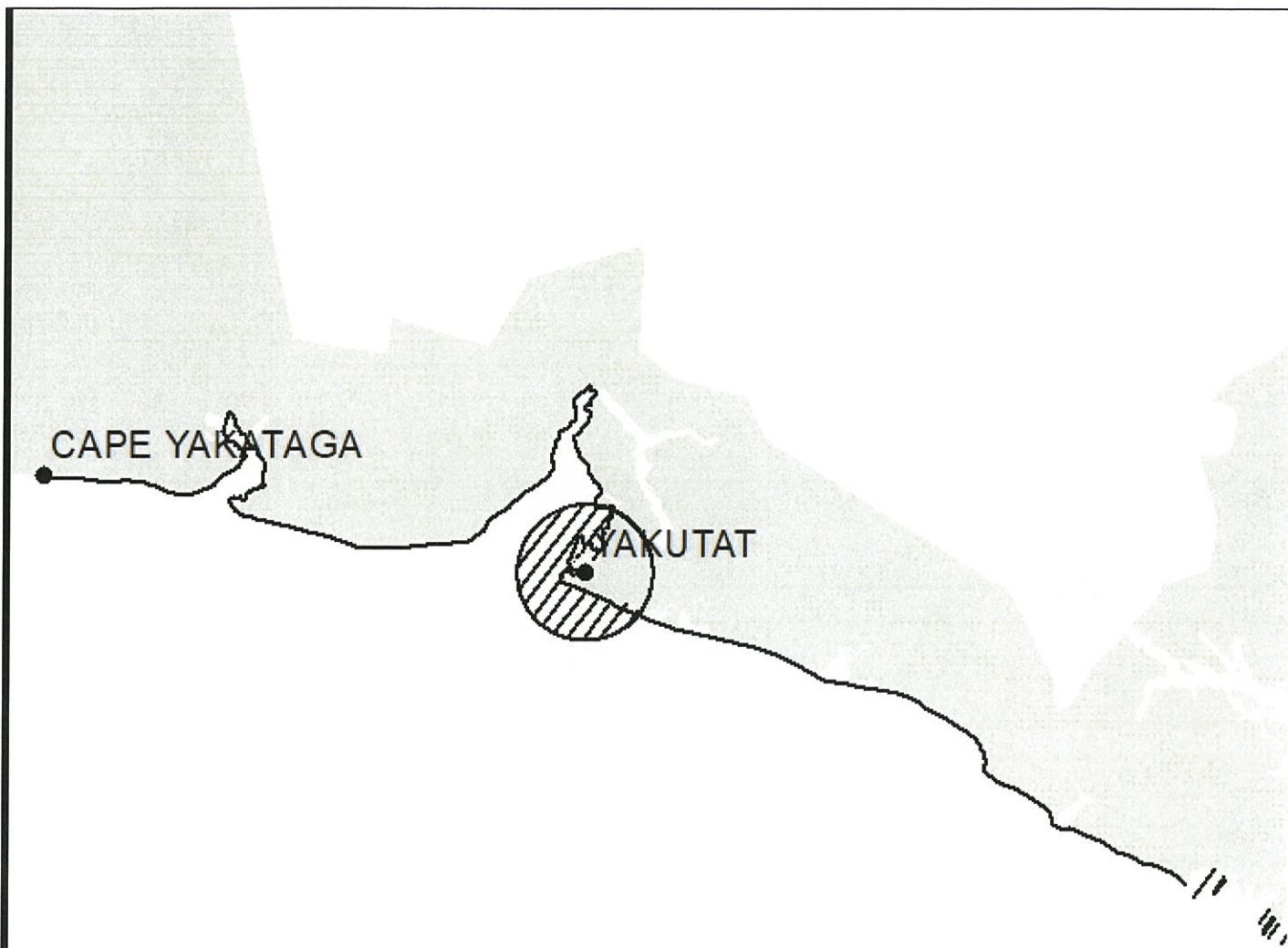
Transects (black lines)
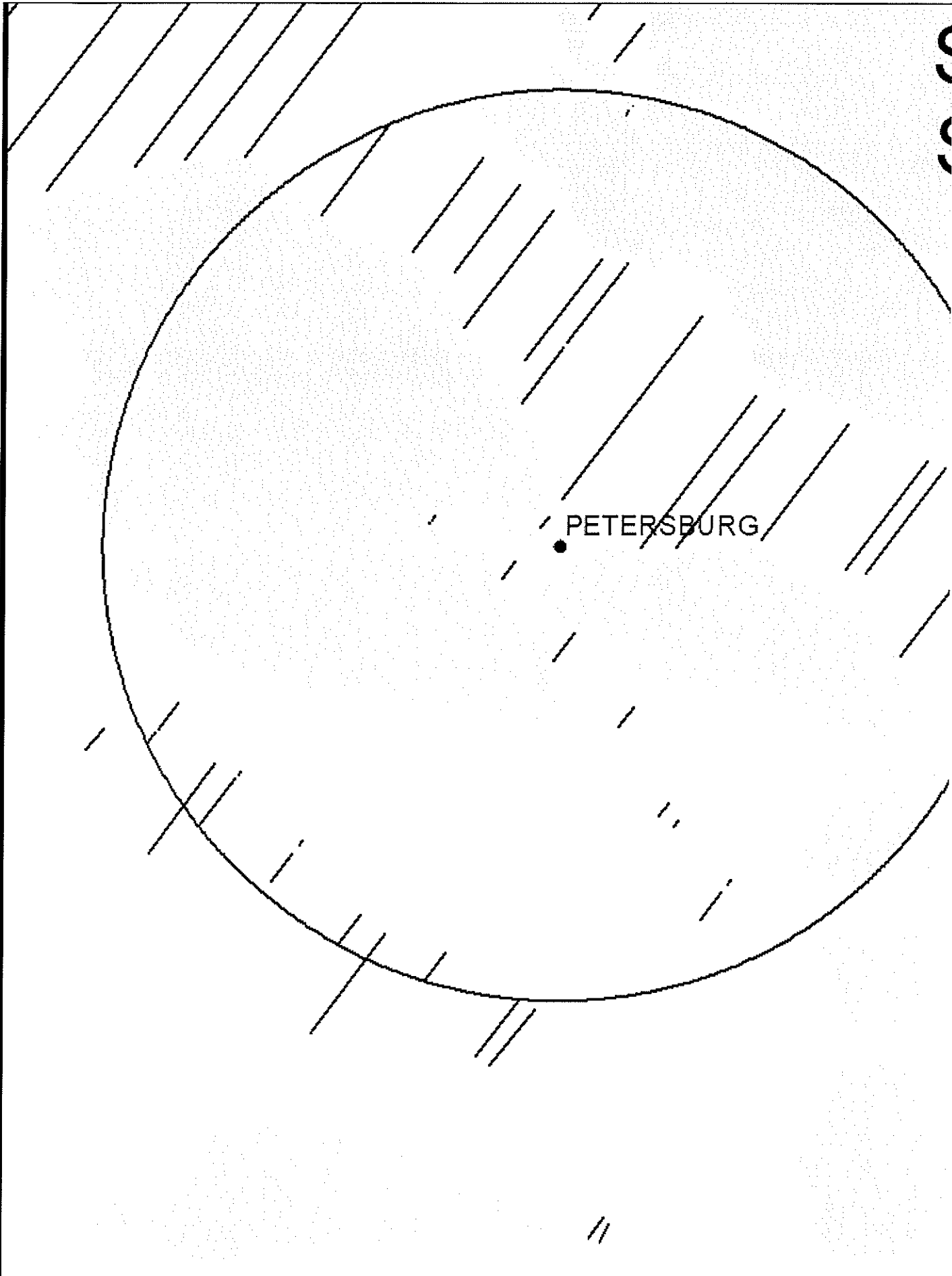Focal Communities (circles)
Glacier Bay (star, to be surveyed by NP

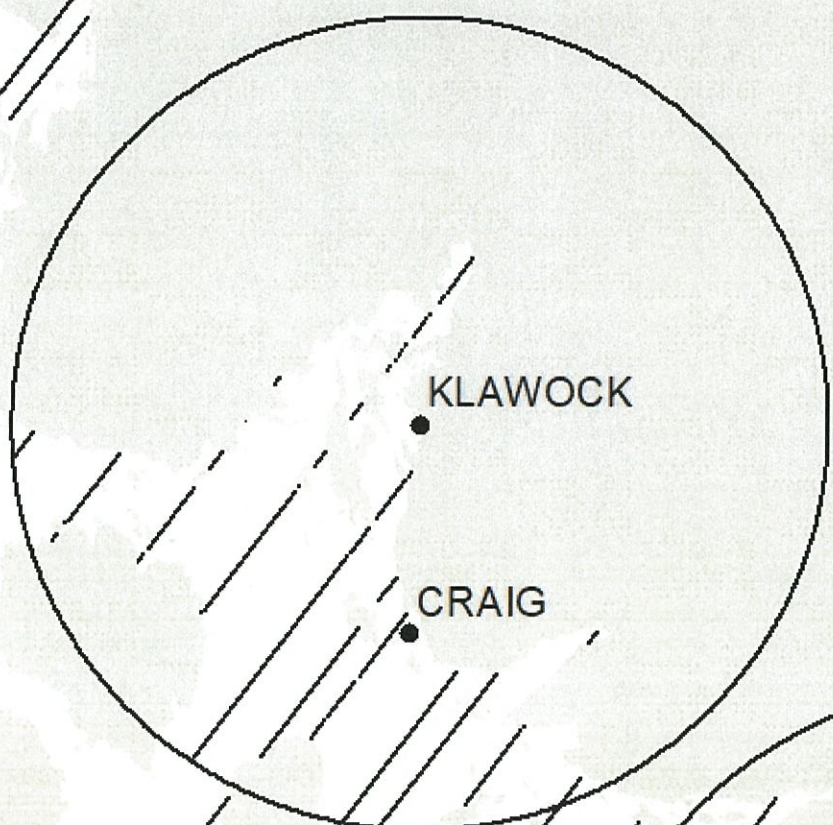# Southeast Alaska Sea Otter Survey 2022

HOONAH

SITKA

PETERSBURG

Southeast Alaska Sea Otter Survey 2022

KLAWOCK

CRAIG

HYDABURG

Statistical Report

Recursive Bayesian computation facilitates adaptive optimal design in ecological studies

Clinton B. Leach [ID],[1,8] Perry J. Williams [ID],[2] Joseph M. Eisaguirre [ID],[2,3] Jamie N. Womble [ID],[4,5] Michael R. Bower,[4] and Mevin B. Hooten[1,6,7]

[1]Department of Fish, Wildlife, and Conservation Biology, Colorado State University, Fort Collins, Colorado 80523 USA
[2]Department of Natural Resources and Environmental Science, University of Nevada, Reno, Nevada 89557 USA
[3]U.S. Fish and Wildlife Service, Marine Mammals Management, Anchorage, Alaska 99503 USA
[4]Southeast Alaska Inventory and Monitoring Network, National Park Service, Juneau, Alaska 99801 USA
[5]Glacier Bay Field Station, National Park Service, Juneau, Alaska 99801 USA
[6]U.S. Geological Survey, Colorado Cooperative Fish and Wildlife Research Unit, Fort Collins, Colorado 80523 USA
[7]Department of Statistics, Colorado State University, Fort Collins, Colorado 80523 USA

Abstract. Optimal design procedures provide a framework to leverage the learning generated by ecological models to flexibly and efficiently deploy future monitoring efforts. At the same time, Bayesian hierarchical models have become widespread in ecology and offer a rich set of tools for ecological learning and inference. However, coupling these methods with an optimal design framework can become computationally intractable. Recursive Bayesian computation offers a way to substantially reduce this computational burden, making optimal design accessible for modern Bayesian ecological models. We demonstrate the application of so-called prior-proposal recursive Bayes to optimal design using a simulated data binary regression and the real-world example of monitoring and modeling sea otters in Glacier Bay, Alaska. These examples highlight the computational gains offered by recursive Bayesian methods and the tighter fusion of monitoring and science that those computational gains enable.

Key words: Bayesian hierarchical modeling; computational efficiency; monitoring; survey design.

Introduction

Ecological science involves both data collection and statistical modeling, but these two fundamental elements are often developed separately and sequentially in practice. Studies are commonly structured based on static random or space-filling designs. These designs have useful properties in some inferential settings, but may not represent the most efficient use of limited field resources, especially in complex, dynamic ecological systems. In fact, dynamically evolving processes may be monitored more efficiently with dynamically evolving designs (Hooten et al. 2009). Such designs can reduce redundancy in data collection (Wikle and Royle 1999) and produce higher

quality data and lower prediction uncertainty (Hooten et al. 2009). Moreover, static surveillance monitoring may not make use of existing ecological knowledge that can lead to improved study designs and inference (Nichols and Williams 2006). In contrast, optimal adaptive survey design recognizes that existing data (e.g., from a pilot study or previous monitoring work) provide ecological information that can be leveraged to ensure that future data collection efforts are set up to be efficient and informative (Wikle and Royle 2005, Hooten et al. 2009).

The optimal design process is iterative, and proceeds through the following steps: collection of data, development and fitting of a statistical model, generation of predictions, evaluation and selection of a new design based on the model and its predictions, collection of new data using that design, and so on (Williams et al. 2018, Hooten et al. 2019). Throughout this process, practitioners are required to make a number of choices. Among these is the choice of model framework and structure.

Hierarchical Bayesian modeling has become widespread in ecology and is particularly well suited to integrating ecological processes with unknown parameters and noisy data (Berliner 1996, Wikle and Hooten 2010). This integration is achieved by specifying three levels of the statistical model (Berliner 1996): the data model that connects observations to the latent ecological process, the process model that describes that ecological process and its associated uncertainty, and parameter models that use prior information to constrain and inform the parameters of the data and process models.

Fitting these hierarchical models is computationally intensive and time consuming, especially for large spatio-temporal models (e.g., requiring more than 10 h in Williams et al. [2018]). Furthermore, evaluating a given design often requires generating predictions of the observations that design might produce in a future data collection effort, augmenting the original data with the predicted data, and fitting the model to the augmented data set. This fitted model then provides a means to evaluate how those new data would affect our understanding of the ecological process and its uncertainty. Finding an optimal design requires repeating this process (i.e., fitting the Bayesian hierarchical model) for every potential design. When the number of potential designs is large, the computational burden of each individual model fit renders this task computationally infeasible, requiring substantial cloud-based or cluster resources (e.g., Williams et al. 2018), or completely intractable.

The computational burden of the hierarchical Bayesian treatment has limited its application in optimal design settings, instead forcing practitioners to rely on other methods (e.g., Kalman filters; Wikle and Royle 2005, Hooten et al. 2009), or explore a relatively limited subset of designs (Williams et al. 2018). Thus, we currently lack the ability to carry the inference offered by modern Bayesian statistical models forward into the design phase without having to make compromises about the designs and models we consider. The main computational bottleneck involves updating an existing posterior distribution with predicted future data, which is the crux of Bayesian optimal adaptive design.

Recursive Bayesian inference provides methods that are well-suited to addressing this bottleneck. In particular, recursive methods enable a statistical model to be fit in a series of steps (e.g., to different groups of data, or to new data as it becomes available; Hooten et al. 2019). This partitioning of the statistical fitting procedure can offer large computational gains over fitting the full model every time new data need to be assimilated (Hooten et al. 2019). Recursive Bayesian methods have recently been used to facilitate computation in complex ecological models (e.g., Hooten et al. 2016, Gerber et al. 2018), but they have yet to be applied in the optimal design setting.

In what follows, we demonstrate how recursive Bayesian methods can be integrated into the optimal design workflow to substantially reduce the computational cost of assimilating new data from each potential design. We

first provide an overview of the optimal design process in a Bayesian hierarchical setting, and identify the crucial role that recursive Bayesian computing can play in reducing the computational burden. Then we demonstrate the recursive Bayes optimal design approach in an application using simulated data and a binary regression framework. Finally, we apply the recursive Bayes optimal design framework to a complex Bayesian hierarchical model of sea otter spatiotemporal dynamics, demonstrating the substantial computational gains that recursive Bayesian methods offer. These examples highlight the important role that recursive Bayesian methods can play in formally coupling optimal adaptive design and modern hierarchical Bayesian modeling, leading to improved ecological inference and closing the feedback loop between modeling and data collection.

METHODS

Evaluating a design

We represent all possible observations of an ecological process of interest as an $N \times 1$ vector $\mathbf{y}$ (e.g., containing abundance or presence/absence at a complete set of sites in a study area). Then, we collect an initial sample of n_1 observations, $\mathbf{y}_1$, produced by an $n_1 \times N$ design matrix $\mathbf{K}_1$ that maps the full domain to the initial observations such that $\mathbf{y}_1 = \mathbf{K}_1 \mathbf{y}$. The design matrix, $\mathbf{K}_1$, is usually a (sparse) matrix composed of zeros and ones that selects the subset of $\mathbf{y}$ that is observed. Given a Bayesian model with parameters $\boldsymbol{\theta}$, we obtain a sample from the first-stage posterior distribution $[\boldsymbol{\theta}|\mathbf{y}_1]$ using an appropriate stochastic sampling algorithm (Gelfand and Smith 1990). Importantly, the recursive Bayes procedure outlined here is compatible with any valid first-stage sampling algorithm (Hooten et al. 2019), including Markov chain Monte Carlo (MCMC) and Hamiltonian Monte Carlo (HMC), and any software implementation thereof (e.g., NIMBLE [de Valpine et al. 2017] or Stan [Carpenter et al. 2016]).

In the optimal design framework, we use the existing data $\mathbf{y}_1$ and the fitted model to compare how different designs for future data collection affect our estimate of some target quantity (often a measure of uncertainty). Formally, we let $l = 1, \ldots, L$ index the set of all possible designs, defined by $n_2 \times N$ design matrices $\mathbf{K}_2^{(l)}$, that would produce a new set of n_2 observations given by $\mathbf{y}_2^{(l)} = \mathbf{K}_2^{(l)} \mathbf{y}$. The first step of optimal design is to define a design criterion, $d^{(l)}\left(\mathbf{y}_1, \mathbf{y}_2^{(l)}\right)$, that summarizes some aspect of our understanding of the process given both the original and the new data. Choices of design criterion often include prediction variance (Hooten et al. 2009) or the variance of model parameters (Hooten et al. 2012) or derived quantities (e.g., abundance; Williams et al. 2018), in which case the goal of optimal design is to find the design that will yield the smallest variance (i.e., the least uncertainty).

Generally, the design criterion will depend either on the posterior predictive distribution of the full process

$$\left[\mathbf{y}\middle|\mathbf{y}_1,\mathbf{y}_2^{(l)}\right] = \int \left[\mathbf{y}\middle|\mathbf{y}_1,\mathbf{y}_2^{(l)},\boldsymbol{\theta}\right][\boldsymbol{\theta}|\mathbf{y}_1,\mathbf{y}_2^{(l)}]d\boldsymbol{\theta}, \qquad (1)$$

or directly on the posterior distribution of the model parameters $\left[\boldsymbol{\theta}\middle|\mathbf{y}_1,\mathbf{y}_2^{(l)}\right]$. In principle, to evaluate the design criterion for a given $\mathbf{K}_2^{(l)}$, we need to measure the process (i.e., observe $\mathbf{y}_2^{(l)}$), augment the existing data with that measurement, and fit the statistical model to characterize $\left[\boldsymbol{\theta}\middle|\mathbf{y}_1,\mathbf{y}_2^{(l)}\right]$ and hence the posterior predictive distribution $\left[\mathbf{y}\middle|\mathbf{y}_1,\mathbf{y}_2^{(l)}\right]$. Thus, computing $d^{(l)}\left(\mathbf{y}_1,\mathbf{y}_2^{(l)}\right)$ given new (predicted) data requires fitting the model to the augmented data, which, in the case of modern Bayesian hierarchical models, may be computationally demanding. If the number of potential designs, L, is large, the standard Bayesian optimal design procedure becomes intractable.

However, we can further decompose the posterior distribution as

$$\begin{aligned}\left[\boldsymbol{\theta}\middle|\mathbf{y}_1,\mathbf{y}_2^{(l)}\right] &\propto \left[\mathbf{y}_2^{(l)}\middle|\mathbf{y}_1,\boldsymbol{\theta}\right]\left[\boldsymbol{\theta}\middle|\mathbf{y}_1\right], \\ &\propto \left[\mathbf{y}_2^{(l)}\middle|\mathbf{y}_1,\boldsymbol{\theta}\right]\left[\mathbf{y}_1\middle|\boldsymbol{\theta}\right]\left[\boldsymbol{\theta}\right],\end{aligned} \qquad (2)$$

where $[\boldsymbol{\theta}|\mathbf{y}_1] \propto [\mathbf{y}_1|\boldsymbol{\theta}][\boldsymbol{\theta}]$ is available from the original model fit to $\mathbf{y}_1$. This natural decomposition of the posterior distribution of $\boldsymbol{\theta}$ makes clear that the first-stage posterior distribution, $[\boldsymbol{\theta}|\mathbf{y}_1]$, serves as a prior on $\boldsymbol{\theta}$ in the second-stage analysis of the augmented data (Hooten et al. 2019). In prior-proposal recursive Bayes (PPRB), we also use $[\boldsymbol{\theta}|\mathbf{y}_1]$ as the proposal distribution in a Metropolis-Hastings MCMC algorithm to update the posterior distribution of $\boldsymbol{\theta}$ given the new data produced by a given design (Hooten et al. 2019).

At step k of the PPRB MCMC algorithm, we sample a proposal $\boldsymbol{\theta}^{(*)} \sim [\boldsymbol{\theta}|\mathbf{y}_1]$. We then accept that proposal and set $\boldsymbol{\theta}^{(k+1)} = \boldsymbol{\theta}^{(*)}$ with probability $\min(1, r)$, where

$$\begin{aligned}r &= \frac{\left[\mathbf{y}_2^{(l)}\middle|\boldsymbol{\theta}^{(*)},\mathbf{y}_1\right]\left[\boldsymbol{\theta}^{(*)}\middle|\mathbf{y}_1\right]}{\left[\mathbf{y}_2^{(l)}\middle|\boldsymbol{\theta}^{(k-1)},\mathbf{y}_1\right]\left[\boldsymbol{\theta}^{(k-1)}\middle|\mathbf{y}_1\right]}\frac{\left[\boldsymbol{\theta}^{(k-1)}\middle|\mathbf{y}_1\right]}{\left[\boldsymbol{\theta}^{(*)}\middle|\mathbf{y}_1\right]}, \\ &= \frac{\left[\mathbf{y}_2^{(l)}\middle|\boldsymbol{\theta}^{(*)},\mathbf{y}_1\right]}{\left[\mathbf{y}_2^{(l)}\middle|\boldsymbol{\theta}^{(k-1)},\mathbf{y}_1\right]},\end{aligned} \qquad (3)$$

where allowing the original posterior distribution to serve as both prior and proposal enables the cancellation and results in a ratio that depends only on the conditional likelihood of the new data. Note that, because we often have a finite MCMC sample from the first model fit (and thus a finite set of proposals, $\boldsymbol{\theta}^{(*)}$, for this stage), we can pre-compute $\left[\mathbf{y}_2^{(l)}\middle|\boldsymbol{\theta}^{(*)},\mathbf{y}_1\right]$ for each design and proposal before the second stage and in parallel (Hooten

et al. 2019). This pre-computation, together with the relative simplicity of the above Metropolis-Hastings ratio, can lead to a substantial decrease in computation time compared to running the full sampling algorithm for every design. Code implementing PPRB for the following examples is available in Data S1 (archived in Leach 2021) and Data S2 (archived in Eisaguirre 2021).

Generating potential future data

The above discussion assumes that $\mathbf{y}_2^{(l)}$ is known, which, of course, it is not. In the case of Gaussian models (e.g., Wikle and Royle 1999), the design criterion $d^{(l)}$ depends only on $\mathbf{K}_2^{(l)}$ and the modeled dependence structure, and thus new data are not required. In more complex models, evaluating the design requires predictions of the new data $\mathbf{y}_2^{(l)}$ (Wikle and Royle 2005). These predictions can be readily generated by draws from the posterior predictive (or imputation) distribution of $\mathbf{y}_2^{(l)}$ produced from the first stage model

$$\left[\mathbf{y}_2^{(l)}\middle|\mathbf{y}_1\right] = \int \left[\mathbf{y}_2^{(l)}\middle|\mathbf{y}_1,\boldsymbol{\theta}\right][\boldsymbol{\theta}|\mathbf{y}_1]d\boldsymbol{\theta}. \qquad (4)$$

We can then use a multiple imputation approach (Rubin 1996, Scharf et al. 2017) to average the design criterion over the imputation distribution such that

$$\begin{aligned}d^{(l)}(\mathbf{y}_1) &= \int d^{(l)}\left(\mathbf{y}_1,\mathbf{y}_2^{(l)}\right)[\mathbf{y}_2^{(l)}|\mathbf{y}_1]d\mathbf{y}_2^{(l)}, \\ &= E\left(d^{(l)}\left(\mathbf{y}_1,\mathbf{y}_2^{(l)}\right)\middle|\mathbf{y}_1\right)\end{aligned} \qquad (5)$$

In practice, we can compute this expectation by first obtaining samples, $\mathbf{y}_2^{(l)(m)} \sim [\mathbf{y}_2^{(l)}|\mathbf{y}_1]$ for $m = 1, \ldots, M$, from the first stage posterior predictive distribution. We then fit the model to each of the M augmented data sets $\left(\mathbf{y},\mathbf{y}_2^{(l)(m)}\right)$, obtain samples from each of the posterior distributions $\left[\boldsymbol{\theta}\middle|\mathbf{y}_1,\mathbf{y}_2^{(l)(m)}\right]$ using PPRB, and compute the mean of the corresponding design criteria:

$$d^{(l)}(\mathbf{y}_1) = \frac{1}{M}\sum_m d^{(l)}\left(\mathbf{y}_1,\mathbf{y}_2^{(l)(m)}\right). \qquad (6)$$

The accuracy of the expectation will improve as M grows larger, but often a relatively small M (on the order of 10) will be sufficient (Rubin 1996).

The multiple imputation procedure enables us to account for the uncertainty in the future data in the evaluation of the design criterion. Alternatively, if accounting for such uncertainty is not desired or necessary, we could generate a single point estimate of future data by computing the posterior predictive mean (or median or mode, as appropriate) of $\left[\mathbf{y}_2^{(l)}\middle|\mathbf{y}_1\right]$ or assigning a single fixed forecast of $\mathbf{y}_2^{(l)}$ from another source (e.g., expert opinion).

Optimization

Given an ability to rapidly compute the design criterion $d^{(l)}$, the optimal design can be obtained by finding the design that minimizes (or maximizes) $d^{(l)}$. In cases where the design space is relatively small, each design can be evaluated and the global optimum selected. If the design space is too large to evaluate every design, an optimization routine may be required (e.g., an exchange algorithm; Royle and Nychka 1998).

EXAMPLE: SIMULATED BINARY REGRESSION

Consider a situation in which we seek to predict the occupancy of a particular species across a spatial domain comprising 100 discrete units (e.g., plots or transects) over which we measure a covariate (e.g., through remote sensing), x_i for $i = 1, \ldots, 100$ (Fig. 1b). Let $\mathbf{y}$ be a vector comprising binary occupancy at all sites. An initial data collection effort randomly samples 10 of these sites, producing initial data set $\mathbf{y}_1 = \mathbf{K}_1\mathbf{y}$ with covariates $\mathbf{x}_1 = \mathbf{K}_1\mathbf{x}$, where $\mathbf{K}_1$ is a 10×100 matrix of zeros and ones, with a single one in each row identifying the sampled plot.

We model these data using binary regression, with a Bernoulli likelihood and a probit link function (Φ^{-1}, the inverse CDF of a standard normal distribution). The resulting full Bayesian model is as follows:

$$
\begin{aligned}
y_{1i} &\sim \text{Bernoulli}(p_i), \\
\Phi^{-1}(p_i) &= \beta_0 + \beta_1 x_{1i}, \\
\beta_0 &\sim \text{Normal}(0, \ \sigma_0^2), \\
\beta_1 &\sim \text{Normal}(0, \ \sigma_1^2).
\end{aligned}
\tag{7}
$$

We use the data augmentation and Gibbs sampling approach of Albert and Chib (1993) to draw an MCMC sample from the posterior distribution of the regression coefficients ($[\beta|\mathbf{y}_1]$) and the posterior predictive distribution of occupancy across the study domain ($[\mathbf{y}|\mathbf{y}_1]$). This posterior sample could alternatively be generated using other algorithms (e.g., HMC) or software (e.g., brms; Bürkner 2017) without changing the following workflow. The goal of the optimal design framework is to use this initial data set and model output to select the next site (of the remaining 90) to be sampled. That is, each of the remaining 90 sites represent a potential design, indexed by l, that corresponds to a 1×100 design vector $\mathbf{K}_2^{(l)}$ that has a single 1 in the position of the sampled site and produces new data $y_2^{(l)} = \mathbf{K}_2^{(l)}\mathbf{y}$.

To select the optimal design, we first specify a design criterion. Our goal is to predict occupancy. Thus we seek the design that minimizes the total posterior predictive variance given both the initial and new data

$$
d^{(l)}\left(\mathbf{y}_1, y_2^{(l)}\right) = \sum_{i=1}^{100} \text{var}(y_i|\mathbf{y}_1, y_2^{(l)}),
\tag{8}
$$

where $\text{var}(y_i|\mathbf{y}_1, y_2^{(l)})$ is the pointwise posterior predictive variance calculated using the MCMC sample from

$\left[y_i \middle| \mathbf{y}_1, y_2^{(l)}\right]$ produced by PPRB. To account for the uncertainty in predictions of the future $y_2^{(l)}$, we average this design criterion over the imputation distribution $\left[y_2^{(l)} \middle| \mathbf{y}_1\right]$ to obtain $d^{(l)}(\mathbf{y}_1)$. In the binary case, imputed realizations $y_2^{(l)(m)}$ can only take on values of 0 or 1, enabling efficient computation of this expectation (see Appendix S1).

Evaluating the design criterion requires sampling from $\left[\beta \middle| \mathbf{y}_1, y_2^{(l)(m)}\right]$ for all 90 designs and imputed future data sets. Rather than fit the model to the entire data set $\left(y_2^{(l)(m)}, \mathbf{y}_1\right)$, we apply PPRB to use the existing output from the initial MCMC algorithm (i.e., the $\beta^{(k)}$ drawn from $[\beta|\mathbf{y}_1]$). At step k of the second-stage MCMC algorithm for design l and imputed data m, we implement PPRB as follows:

1) Sample a proposal $\beta^{(*)} \sim [\beta|\mathbf{y}_1]$ (i.e., selected randomly with replacement from the first stage MCMC sample).
2) Compute the PPRB Metropolis-Hastings ratio

$$
r = \frac{\left[y_2^{(l)(m)} \middle| \beta^{(*)}\right]}{\left[y_2^{(l)(m)} \middle| \beta^{(k)}\right]}.
\tag{9}
$$

3) Accept the proposal $\beta^{(*)}$ with probability $\min(r, 1)$.

Using the second-stage samples $\beta^{(k)}$, we compute the design criteria for each potential design (averaging over the imputation distribution) and identify the optimal site for the next sample (Fig. 1c, d). The expected design criterion is largest (i.e., with the largest predictive variance) for sites with more extreme covariate values (Fig. 1c). Despite the fact that the inflection point (i.e., the x value where $p(x) = 0.5$) represents the largest Bernoulli variance, sampling locations with covariate values slightly larger than this inflection point produce the smallest total expected prediction variance. The positioning of the optimal design just off the inflection point highlights the fact that, even in simple models, the optimal design is often not intuitive and justifies the need for rigorous optimal design in ongoing ecological monitoring. In more complex spatiotemporal models, often with larger design spaces, it becomes even more difficult to identify effective designs a priori (Wikle and Royle 1999, 2005), further emphasizing the need for PPRB and the speed with which it enables us to evaluate a potentially large number of designs.

EXAMPLE: SPATIOTEMPORAL DYNAMICS

Sea otters (*Enhydra lutris*) are an apex predator of the nearshore marine community of the North Pacific Ocean and nearly went extinct at the turn of the 20th century. Reintroductions, translocations, and legal

protections allowed sea otters to recolonize much of their former range (Williams et al. 2019). The return of sea otters has influenced marine food webs, both directly and indirectly, with impacts on commercially important fisheries. Thus, information regarding the continued growth and expansion of sea otters is critical for predicting future expansion, understanding their role as a keystone species, and for informing natural resource management (Tinker et al. 2019). Sea otters are surveyed using aircraft over large spatial domains and flight time is typically restricted by range and fuel capacity of aircraft and operating conditions (Williams et al. 2017a). Sampling designs must balance requisite data collection with human safety, aircraft availability, and cost.

To estimate growth and colonization dynamics of sea otters in Glacier Bay, Alaska, Williams et al. (2017b)

developed a mechanistically motivated reaction-diffusion model known as ecological diffusion, embedded within a Bayesian hierarchical framework with data, process, and parameter levels (sensu Berliner 1996). This model was fit to sea otter aerial survey counts (Esslinger 2019), with data and process models specified as follows

$$
\begin{aligned}
\text{Data Model} : y_t(\mathbf{s}_i) &\sim \text{Binomial}(n_t(\mathbf{s}_i), \phi), \\
\text{Process Model} : n_t(\mathbf{s}_i) &\sim \text{Poisson}(u(\mathbf{s}_i, t)), \\
\frac{\partial u(\mathbf{s}, t)}{\partial t} &= \left(\frac{\partial^2}{\partial s_1^2} + \frac{\partial^2}{\partial s_2^2} \right) [\mu(\mathbf{s}, t) u(\mathbf{s}, t)] + \gamma u(\mathbf{s}, t).
\end{aligned}
\tag{10}
$$

In Eq. 10, $y_t(\mathbf{s}_i)$ represents sea otter count data at locations $\mathbf{s}_i$ for $i = 1, \ldots, J$ during time t, $n_t(\mathbf{s}_i)$ is the
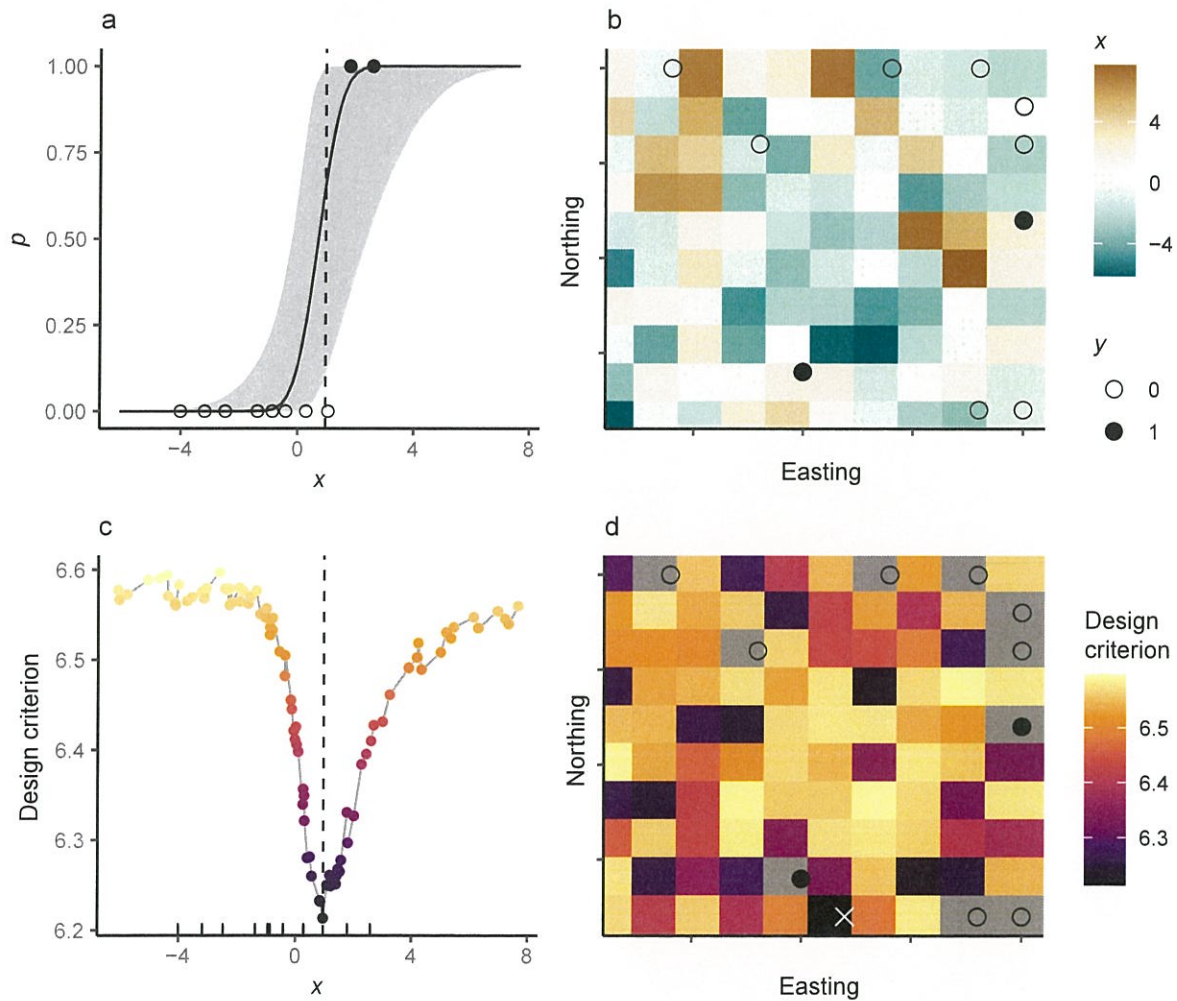

Fig. 1. Initial data collection effort and evaluation of the optimal design for a binary regression model. (a) The initial estimated occupancy probability p as a function of x, with the black line showing the posterior median and the gray ribbon showing the 95% credible interval. The points show the data obtained from (b) an initial random survey of the study domain. In panel b, each square is a sampling plot with measured covariate x indicated by the color of the fill. The points indicate the initial sites surveyed, with filled circles indicating the organism was present and open circles indicating absence. Each of the remaining plots represent a potential design for the next survey. (c, d) The computed design criteria for each of the 90 potential designs as a function of the x value at each plot (c) and mapped on the study domain (d). The dashed line in panels a and c indicates the x value of the optimal plot and the white × identifies the optimal plot in panel d.

true latent abundance of sea otters, and ϕ is the individual sea otter detection probability. The dynamic abundance intensity process, $u(\mathbf{s}, t)$, was governed by an ecological diffusion PDE, with a constant instantaneous Malthusian growth γ and motility $\mu(\mathbf{s}, t)$ modeled as a function of spatially varying covariates. See Appendix S1 for the full model specification. The model described in Eq. 10 was fit to baseline data, $\mathbf{y}_1$ collected for $t = 1993, \ldots, 2012$, using a custom MCMC algorithm (Williams et al. 2017b). We used our algorithm to obtain three MCMC chains in parallel, with 50,000 draws per chain plus 10,000 for burn in. This required approximately 5 h per chain, for a total of 15 CPU hours.

Following the optimal design framework, our goal was to use the initial data $\mathbf{y}_1$ and corresponding model output to inform the collection of transects to be surveyed in a hypothetical 2013, producing new data $\mathbf{y}_2^{(l)}$. Rather than choosing a design criterion based on the posterior predictive density as in the binary regression example, in this example, we focused on the latent total abundance intensity in 2013, $u_{2013} = \int_S u_{2013}(\mathbf{s})d\mathbf{s}$. Our objective was to minimize the variance of the total intensity $d^{(l)}\left(\mathbf{y}_1, \mathbf{y}_2^{(l)}\right) = \mathrm{var}\left(u_{2013} \big| \mathbf{y}_1, \mathbf{y}_2^{(l)}\right)$, where $\mathrm{var}(u_{2013} \big| \mathbf{y}_1, \mathbf{y}_2^{(l)})$ is the predictive process variance calculated using the MCMC sample from $[u_{2013}|\mathbf{y}_1, \mathbf{y}_2^{(l)}]$ produced by PPRB. We used the multiple imputation approach described above to average this design criterion over the posterior predictive distribution of $\mathbf{y}_2^{(l)}$ using $M = 100$ draws of $\mathbf{y}_2^{(l)(m)} \sim \left[\mathbf{y}_2^{(l)}\big|\mathbf{y}_1\right]$, such that

$$d^{(l)}(\mathbf{y}_1) \approx \frac{1}{M} \sum_{m=1}^{M} \mathrm{var}(u_{2013}|\mathbf{y}_1, \mathbf{y}_2^{(l)(m)}). \qquad (11)$$

For each design l and imputed future data set m, we implemented the PPRB MCMC algorithm as follows:

1) Sample a proposal $\left(\mathbf{n}_{2013}^{(*)}, \mathbf{u}_{2013}^{(*)}\right) \sim [\mathbf{n}_{2013}, \mathbf{u}_{2013}|\mathbf{y}_1]$.
2) Compute the PPRB Metropolis-Hastings ratio

$$r = \frac{\left[\mathbf{y}_2^{(l)(m)}\Big|\mathbf{n}_{2013}^{(*)}\right]}{\left[\mathbf{y}_2^{(l)(m)}\Big|\mathbf{n}_{2013}^{(k)}\right]}. \qquad (12)$$

3) Accept the proposal $\left(\mathbf{n}_{2013}^{(*)}, \mathbf{u}_{2013}^{(*)}\right)$ with probability $\min(r, 1)$.

From the resulting MCMC chains, we computed $d^{(l)}$ for each candidate design. Given constraints associated with aircraft range and availability, approximately 20 transects can be flown per day in Glacier Bay, resulting in $\left(\frac{170}{20}\right)$ possible survey designs given the dimensions of the survey area and the resolution of the data collection methods (Williams et al. 2018). While it was not feasible to assess all possible designs, the PPRB procedure allowed us to compare many more than was previously practical. Given that the ecological diffusion model required approximately 15 CPU hours to estimate parameters using an MCMC algorithm, previous optimization routines that fit the model for each design using MCMC would require 1500 CPU hours to assess just 1 design over 100 imputed data sets (Williams et al. 2018). In contrast, the PPRB approach permitted us to compute the design criterion of 1,000 designs (Fig. 2a) in about 480 CPU hours, which we reduced to <5 h of run time by parallelizing evaluation over multiple CPUs. The survey design that optimized our design criterion (Fig. 2b) reduced the variance of the hypothetical 2013 sea otter abundance estimate by 38% over the average random design.

DISCUSSION

Applying the principles of optimal design to make efficient use of field resources requires methods that make efficient use of computational resources. This is especially true for ecological studies in which Bayesian hierarchical models are deployed. These models can capture rich mechanistic information (Wikle and Hooten 2010) but are often computationally demanding to fit. We proposed the use of PPRB (Hooten et al. 2019) to alleviate the computational burden and make evaluating a large number of designs feasible. We demonstrated this method using a binary regression model and highlighted that optimal designs may not always be intuitive without a comprehensive search of the design space (Wikle and Royle 1999, 2005). Furthermore, we applied the procedure to a complex Bayesian hierarchical model of sea otter spatiotemporal dynamics and demonstrated the substantial computational gains that PPRB produces relative to fitting the entire model for every considered design and possible data set.

The rapid and relatively extensive search of the design space allowed us to identify a collection of transects for a hypothetical 2013 sea otter aerial survey that would produce a more precise estimate of the total sea otter abundance in Glacier Bay than the average random design. Given that sea otters are a keystone species (Estes and Palmisano 1974) with a rapidly expanding range and abundance in Glacier Bay (Williams et al. 2019), accurately estimating their abundance is crucial for monitoring and conserving the nearshore ecosystem in the face of environmental and anthropogenic changes (Coletti et al. 2016, Tinker et al. 2019). We demonstrated that the optimal design framework, by leveraging existing knowledge of sea otter dynamics, learned through the combination of existing survey data and the mechanistic principles embedded in the reaction-diffusion PDE, can help make monitoring data as useful

a

b
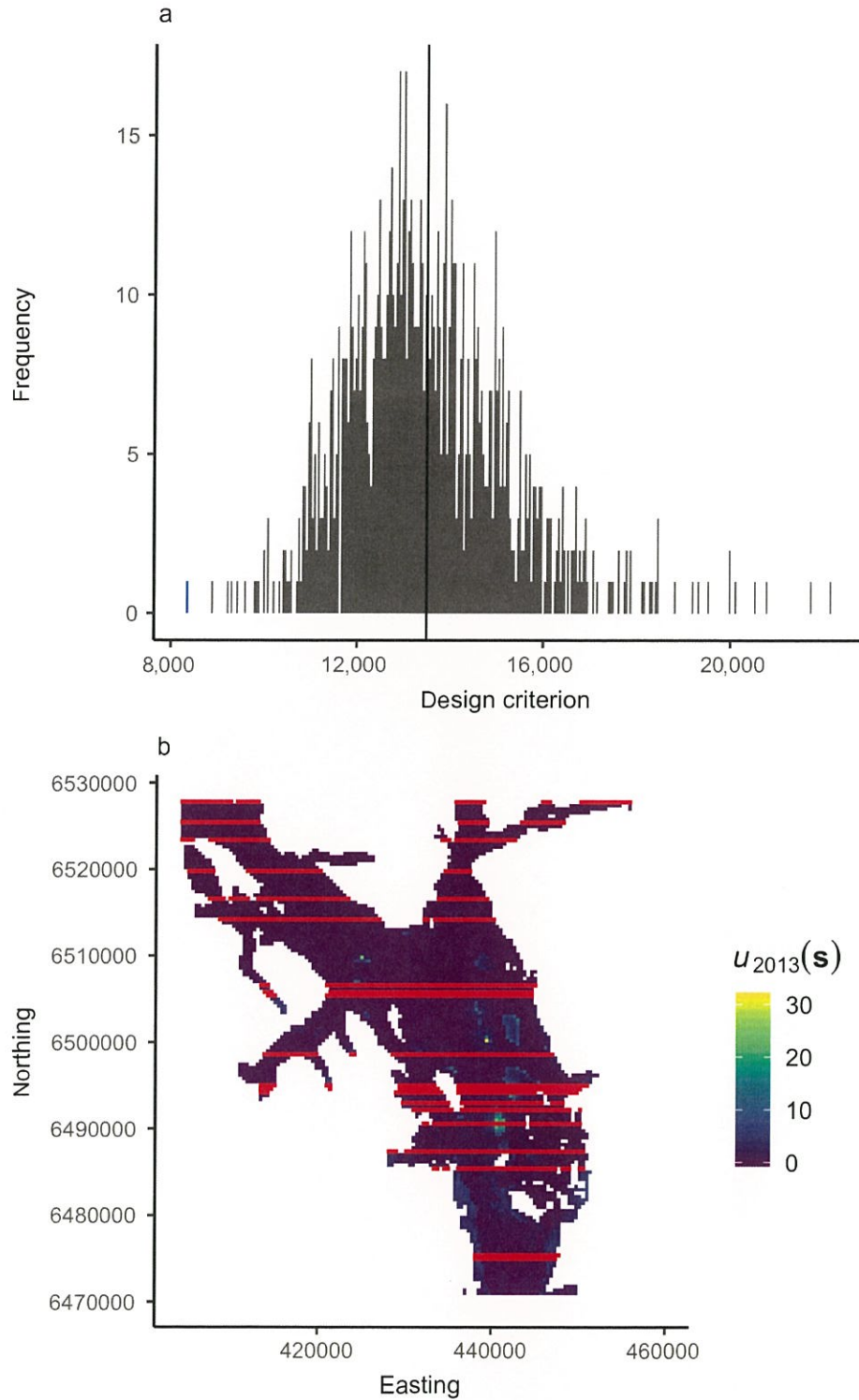
FIG. 2. (a) Histogram of design criteria computed for 1,000 randomly selected sea otter survey designs. The mean is given by the black line and the blue bar indicates the optimal survey design. Each design consisted of 20 transects to be flown over Glacier Bay in southeastern Alaska. (b) Forecasted sea otter abundance intensity across Glacier Bay in 2013, $u_{2013}(s)$, and optimal hypothetical survey design. Red lines correspond to the 20 transects representing the optimal design.

and informative as possible (Nichols and Williams 2006).

The challenges inherent in monitoring sea otters in Glacier Bay and across the North Pacific—costly data collection, dynamic spatiotemporal processes, and the need for quality data for conservation, management, and inference—are emblematic of the challenges faced throughout much of ecology. Both optimal design and Bayesian hierarchical modeling offer potential solutions to some of these challenges, and the use of PPRB allows them to be coupled more easily. This coupling will help to make the optimal design framework accessible to larger monitoring efforts across broader spatial domains and, in particular, may assist in the targeting of monitoring efforts across the sea otter range in the North Pacific (Eisaguirre et al. 2021).

Further, by reducing the computational burden of evaluating a given design, PPRB allows for greater flexibility in implementing the other components of the iterative optimal design framework, including the types of the data collected, the choice of design criteria, and the optimization framework. We focused on applications where the goal was to choose the locations at which to collect a single type of data, but the PPRB optimal design framework could be extended to target sampling across multiple data types (e.g., in integrated population modeling [Schaub et al. 2007] or multispecies studies). Further, we demonstrated two choices of design criterion based on predictive variance (in the binary regression example) and the variance of latent derived quantities (in the sea otter example). The choice of design criterion will depend on the goals of a particular study and could include other components, such as the costs of implementing a given design (Williams and Brown 2020), the benefits of any connected management actions (Williams and Brown 2020), or a measure of the strength of preferential sampling implied by a design (Diggle et al. 2010, Gelfand and Shirota 2019). Last, the approach we described can be enhanced by additional optimization strategies. The speed gains offered by PPRB may make the application of optimization frameworks (e.g., exchange algorithms, Royle and Nychka 1998) more feasible, and the identification of a global optimum more likely.

As we have demonstrated in our examples and discussion, recursive Bayesian methods offer to substantially ease the computational burden of coupling optimal design procedures with Bayesian hierarchical modeling. By facilitating this coupling, recursive Bayesian methods help close the feedback loop between data collection and data analysis, allowing the knowledge produced by Bayesian hierarchical modeling to inform monitoring efforts that improve and accelerate ecological learning and inference.

LITERATURE CITED

Albert, J. H., and S. Chib. 1993. Bayesian analysis of binary and polychotomous response data. Journal of the American Statistical Association 88:669–679.

Berliner, L. M. 1996. Hierarchical Bayesian time series models. Pages 15–22 in K. M. Hanson, and R. N. Silver, editors. Maximum entropy and Bayesian methods. Springer Netherlands, Dordrecht, the Netherlands.

Bürkner, P.-C. 2017. brms: an R package for Bayesian multilevel models using Stan. Journal of Statistical Software 80:1–28.

Carpenter, B., A. Gelman, M. Hoffman, D. Lee, B. Goodrich, M. Betancourt, M. A. Brubaker, P. Li, and A. Riddell. 2016. Stan: a probabilistic programming language. Journal of Statistical Software 76:1–32.

Coletti, H. A., J. L. Bodkin, D. H. Monson, B. E. Ballachey, and T. A. Dean. 2016. Detecting and inferring cause of change in an Alaska nearshore marine ecosystem. Ecosphere 7:e01489.

de Valpine, P., D. Turek, C. J. Paciorek, C. Anderson-Bergman, D. T. Lang, and R. Bodik. 2017. Programming with models: Writing statistical algorithms for general model structures with nimble. Journal of Computational and Graphical Statistics 26:403–413.

Diggle, P. J., R. Menezes, and T. Su. 2010. Geostatistical inference under preferential sampling. Journal of the Royal Statistical Society: Series C (Applied Statistics) 59:191–232.

Eisaguirre, J. M. 2021. jmeisaguirre/glba optimal design (v1.0.0). Zenodo. https://doi.org/10.5281/zenodo.5172817

Eisaguirre, J. M., P. J. Williams, X. Lu, M. L. Kissling, W. S. Beatty, G. G. Esslinger, J. N. Womble, and M. B. Hooten. 2021. Diffusion modeling reveals effects of multiple release sites and human activity on a recolonizing apex predator. Movement Ecology 9:1–14.

Esslinger, G. 2019. Sea otter aerial survey data from Glacier Bay National Park and Preserve, 1999–2012. U.S. Geological Survey data release. https://doi.org/10.5066/P9SBAFF6

Estes, J. A., and J. F. Palmisano. 1974. Sea otters: their role in structure nearshore communities. Science 185:1058–1060.

Gelfand, A. E., and S. Shirota. 2019. Preferential sampling for presence/absence data and for fusion of presence/absence data with presence-only data. Ecological Monographs 89:1–17.

Gelfand, A. E., and A. F. M. Smith. 1990. Sampling-based approaches to calculating marginal densities. Journal of the American Statistical Association 85:398–409.

Gerber, B. D., M. B. Hooten, C. P. Peck, M. B. Rice, J. H. Gammonley, A. D. Apa, and A. J. Davis. 2018. Accounting for location uncertainty in azimuthal telemetry data improves ecological inference. Movement Ecology 6:14.

Hooten, M. B., F. E. Buderman, B. M. Brost, E. M. Hanks, and J. S. Ivan. 2016. Hierarchical animal movement models for population-level inference. Environmetrics 27:322–333.

Hooten, M. B., D. S. Johnson, and B. M. Brost. 2019. Making recursive Bayesian inference accessible. American Statistician 75:185–194

Hooten, M. B., B. E. Ross, and C. K. Wikle. 2012. Optimal spatio-temporal monitoring designs for characterizing population trends. Pages 443–459 in R. A. Gitzen, J. J. Millspaugh, A. B. Cooper, and D. S. Licht, editors. Design and analysis of

long-term ecological monitoring studies. Cambridge University Press, Cambridge, Massachusetts, USA.

Hooten, M. B., C. K. Wikle, S. L. Sheriff, and J. W. Rushin. 2009. Optimal spatio-temporal hybrid sampling designs for ecological monitoring. Journal of Vegetation Science 20:639–649.

Leach, C. B. 2021. Simulated data example of recursive Bayesian computing for optimal design (v1.0.0). Zenodo. https://doi.org/10.5281/zenodo.5172768

Nichols, J. D., and B. K. Williams. 2006. Monitoring for conservation. Trends in Ecology and Evolution 21:668–673.

Royle, J. A., and D. Nychka. 1998. An algorithm for the construction of spatial coverage designs with implementation in SPLUS. Computers and Geosciences 24:479–488.

Rubin, D. B. 1996. Multiple Imputation after 18+ Years. Journal of the American Statistical Association 91:473–489.

Scharf, H., M. B. Hooten, and D. S. Johnson. 2017. Imputation approaches for animal movement modeling. Journal of Agricultural, Biological, and Environmental Statistics 22:335–352.

Schaub, M., O. Gimenez, A. Sierro, and R. Arlettaz. 2007. Use of integrated modeling to enhance estimates of population dynamics obtained from limited data. Conservation Biology 21:945–955.

Tinker, M. T., V. A. Gill, G. G. Esslinger, J. Bodkin, M. Monk, M. Mangel, D. H. Monson, W. W. Raymond, and M. L. Kissling. 2019. Trends and carrying capacity of sea otters in southeast Alaska. Journal of Wildlife Management 83:1073–1089.

Wikle, C. K., and M. B. Hooten. 2010. A general science-based framework for dynamical spatio-temporal models. Test 19:417–451.

Wikle, C. K., and J. A. Royle. 1999. Space-time dynamic design of environmental monitoring networks. Journal of Agricultural, Biological, and Environmental Statistics 4:489–507.

Wikle, C. K., and J. A. Royle. 2005. Dynamic design of ecological monitoring networks for non-Gaussian spatio-temporal data. Environmetrics 16:507–522.

Williams, B. K., and E. D. Brown. 2020. Scenarios for valuing sample information in natural resources. Methods in Ecology and Evolution 11:1534–1549.

Williams, P. J., M. B. Hooten, G. G. Esslinger, J. N. Womble, J. L. Bodkin, and M. R. Bower. 2019. The rise of an apex predator following deglaciation. Diversity and Distributions 25:895–908.

Williams, P. J., M. B. Hooten, J. N. Womble, and M. R. Bower. 2017a. Estimating occupancy and abundance using aerial images with imperfect detection. Methods in Ecology and Evolution 8:1679–1689.

Williams, P. J., M. B. Hooten, J. N. Womble, G. G. Esslinger, and M. R. Bower. 2018. Monitoring dynamic spatio-temporal ecological processes optimally. Ecology 99:524–535.

Williams, P. J., M. B. Hooten, J. N. Womble, G. G. Esslinger, M. R. Bower, and T. J. Heey. 2017b. An integrated data model to estimate spatiotemporal occupancy, abundance, and colonization dynamics. Ecology 98:328–336.

Statistical Report

Improving Wildlife Population Inference Using Aerial Imagery and Entity Resolution

Xinyi Lu, Mevin B. Hooten, Andee Kaplan, Jamie N. Womble, and Michael R. Bower

Recent technological advancements have seen a rapid growth in the use of imagery data to estimate the abundance and spatial distribution of animal populations. However, the value of imagery data may not be fully exploited under traditional analytical frameworks. We developed a method that leverages aerial imagery data for population modeling through entity resolution, a technique that stochastically links the same individual across multiple images. Resolving duplicate individuals in overlapping images that are distorted requires realigning observed point patterns optimally; however, popular machine learning algorithms for image stitching do not often account for alignment uncertainty. Moreover, duplicated individuals can provide insight about detection probability when overlaps are viewed as replicate surveys. Our model resolves individual identities by linking observed locations to latent activity centers and estimates total population as informed by the linkage structure. We developed a hierarchical framework to achieve entity resolution and abundance estimation cohesively, thereby avoiding single-direction error propagation that is common in two-stage models. We illustrate our method through simulation and a case study using aerial images of sea otters in Glacier Bay, Alaska.

Supplementary materials accompanying this paper appear on-line

Key Words: Bayesian; Data augmentation; Hierarchical model; Spatial capture-recapture.

1. INTRODUCTION

Aerial surveys are widely used to provide abundance information about terrestrial and marine species (Caughley 1974; Ver Hoef 2014). Compared to traditional observer-based surveys, imagery surveys have the advantage of reducing risk for observers and providing a permanent record that can be independently verified (Buckland et al. 2012). In addition to

---

X. Lu (✉)· A. Kaplan, Department of Statistics, Colorado State University, Fort Collins, CO 80523, USA (E-mail: *xinyi.lu@colostate.edu*). M. B. Hooten · M. R. Bower, Department of Statistics and Data Sciences, The University of Texas at Austin, Austin, TX 78705, USA. J. M. Womble · M. R. Bower, Southeast Alaska Inventory and Monitoring Network, National Park Service, 3100 National Park Rd, Juneau, AK 99801, USA. J. M. Womble, Glacier Bay Field Station, National Park Service, 3100 National Park Rd, Juneau, AK 99801, USA.

Published online: 12 January 2022

population counts, the imagery data (often referred to as photographs; Fig. 3 in Supplementary Material) provide individual-level information such as color, size, and location, which can be leveraged to identify animals without marking them (Williams et al. 2020). This gain in information leads to more reliable modeling of population abundance than using count data only (Dennis et al. 2015; Barker et al. 2018; Ketz et al. 2019). In what follows, we describe a Bayesian hierarchical model to identify unique individuals in overlapping images and estimate population size under a unified framework. We apply our model to analyze aerial imagery data of sea otters (*Enhydra lutris kenyoni*) in Glacier Bay, Alaska. During a survey, images are acquired at a regular time interval with overlapping regions in the direction of aircraft movement as it flies along transects that are systematically placed across the Glacier Bay. Sea otters in the images are located and counted by trained observers after the survey. Past studies using these data have either discarded overlapping images to meet the independent count assumption of binomial models (Lu et al. 2019), or treated counts from overlapping regions as temporal replicates in N-mixture models (Williams et al. 2017). We demonstrate the advantages of our method over the previously described methods in simulation.

The information we use to resolve individual identities are the observed locations of individuals in a sequence of images. However, individual positions may be distorted when the aircraft deviates from its scheduled trajectory due to a variety of reasons that can influence altitude and aircraft position, resulting in an artificial transformation of the image footprints. Further, micro-movement of sea otters and locating uncertainty during laboratory processing make exact matching of observed locations in overlapping regions nearly impossible. There exists a rich literature on image stitching where the common objective is to optimally combine a sequence of overlapping images into a composite image by minimizing a loss function (Levin et al. 2004; Szeliski 2006; Brown and Lowe 2015; Gross and Heumann 2016). However, optimization-based image stitching algorithms do not usually provide uncertainty about the stitching process and are seldom integrated into other models to provide additional learning about the system. On the other hand, the statistical literature associated with entity resolution, also known as record linkage when the objective is to merge multiple data files (in our case, images) in the absence of unique identifiers (in our case, individual tags, for example), may provide a theoretical basis for uncertainty quantification. We incorporate uncertainty in the record linkage process into a capture-recapture model for abundance estimation.

Traditional approaches to record linkage compare similarities between pairs of records from which matching decisions are made (Fellegi and Sunter 1969; Jaro 1989; Winkler 1995). Larsen and Rubin (2001) presented record linkage as a mixture of linkage probabilities between a model for probable links and a model for probable nonlinks. Fortini et al. (2001), McGlincy (2004), and Larsen (2004) developed the Bayesian approaches based on the same idea. However, comparison-based approaches are largely infeasible computationally, even when the number of possible links is moderately large (Winkler 2006). One way to reduce the computation cost of record linkage is by "blocking," where records partitioned into different blocks are considered nonlinks *a priori* (Christen 2011; Steorts et al. 2014). Alternatively, record linkage can be presented as the clustering of observed records by unobserved identities (Copas and Hilton 1990; Tancredi and Liseo 2011; Liseo and Tan-

credi 2011; Steorts et al. 2015; Tancredi et al. 2018). Each latent identity has a "true" value and the associated records are modeled as stochastic distortions from the truth. Steorts et al. (2015) introduced the graphical record linkage model by representing the linkage structure as a bipartite graph between observed records and latent identities. By comparing records to latent identities instead of each other, the computation time to link d data files with a maximum of n records per file can be substantially reduced from $\mathcal{O}\left(n^d\right)$ to $\mathcal{O}(dn)$. One distinction between the graphical record linkage model and other non-parametric clustering methods such as Dirichlet process models and Pitman-Yor process models is that the latter often assume linear growth of cluster size with the size of data (Wallach et al. 2010; Betancourt et al. 2016), whereas in record linkage problems, co-referent clusters tend to stay small even when the number of records grows. Following Liseo and Tancredi (2011) and Steorts et al. (2015), we made use of a bivariate Gaussian model conditional on the latent truths to identify unique individuals in the imagery data.

The output of a record linkage model can be used to learn about population size. When uncertainty exists in linkage structure, record linkage and size estimation are often regarded as two separate stages (LaPorte et al. 1993; Anderson and Fienberg 1999; Lum et al. 2013). Sadinle (2018) proposed using "linkage-averaging" to transfer linkage uncertainty as quantified by Bayesian posterior samples into the subsequent stage of population size estimation. Although linkage-averaging facilitates model exploration by allowing the combination of different record linkage models with population models, any bias in the record linkage stage will propagate into the size estimation stage regardless of model choice (Tancredi and Liseo 2011). Our hierarchical framework naturally relates entity resolution and abundance estimation as one generative process, thereby allowing information exchange and feedback between these two model objectives. Other unified modeling approaches exist, including those presented by Link et al. (2009) and Wright et al. (2009) that incorporate misidentification into capture-recapture models by sampling from latent multinomial distributions, the hierarchical record linkage models proposed by Tancredi and Liseo (2011) and Liseo and Tancredi (2011) that reflect capture-recapture dynamics through latent matching matrices, and the latent Poisson process model proposed by Green and Mardia (2005) to align partially labeled protein structures. We propose a novel framework that combines a record linkage model and a spatial capture-recapture model (Royle and Young 2008) to align distorted animal locations and to account for heterogeneity in detection probability due to temporally changing survey units.

We present our hierarchical record linkage model in Sect. 2. In Sect. 3, we illustrate the model through simulation and a case study using aerial photographs of sea otters in Glacier Bay, Alaska. Finally in Sect. 4, we discuss possible extensions and broader applications of our model.

2. MODEL

2.1. DATA MODEL

Consider a sequence of T images with n_t observed individuals in image t, for $t = 1, \ldots, T$ (see Fig. 2 in Supplementary Material, for example). Let $\mathbf{y}_{i,t}$ be a two-dimensional

vector of latitude and longitude denoting the observed location of the ith individual in image t, and let $u_{i,t}$ denote the true location of that individual. Distortion in $y_{i,t}$ occurs in laboratory processing when the image footprint, $\mathcal{F}_t$, is artificially scaled and rotated to fit in a template, $\mathcal{Q}_t$, assuming the aircraft trajectory follows a fixed height and orientation. The image centers (latitude, longitude) were recorded by a GPS device on the aircraft in real time and are reliable to represent the truth. Using the known image center μ_t as a reference point, we connect the distorted displacement of the observed location from the image center to that of the true location, $u_{i,t}$, from the image center as

$$y_{i,t} - \mu_t = (1 + c_t)\, R\,(\theta_t)\,\left(u_{i,t} - \mu_t\right), \tag{1}$$

where the counterclockwise rotation matrix is given by

$$R\,(\theta_t) = \begin{pmatrix} \cos\theta_t & -\sin\theta_t \\ \sin\theta_t & \cos\theta_t \end{pmatrix}.$$

The scaling parameter, c_t, and the rotation parameter, θ_t, are modeled using basis function regression to ensure smoothness and flexibility in the aircraft trajectory (Hefley et al. 2017). We specify

$$\begin{aligned} c_t &= w(t)'\alpha, \\ \theta_t &= v(t)'\beta, \end{aligned} \tag{2}$$

where $w(t)$ and $v(t)$ are the basis functions evaluated at time t for scaling and rotation, respectively. Due to unknown distortion, the true image footprints are also unknown, and we model the four vertices of the rectangular image footprint $\mathcal{F}_t$ through a georectification process from the known template $\mathcal{Q}_t$,

$$v_{j,t} - \mu_t = \frac{1}{(1 + c_t)} R\,(-\theta_t)\left(v_{j,t}^* - \mu_t\right), \quad j = 1, 2, 3, 4, \tag{3}$$

where $v_{j,t}$ denote the vertices of $\mathcal{F}_t$ and $v_{j,t}^*$ denote the vertices of $\mathcal{Q}_t$.

We assume every observed individual has a latent identity, $\lambda_{i,t}$, that may be shared across images but not within the same image. The true locations, $u_{i,t}$, are modeled as Gaussian conditioned on a transient activity center associated with the latent identity, $s_{\lambda_{i,t}}$, and movement uncertainty, $\sigma_u^2 I$, such that

$$u_{i,t}|s_{\lambda_{i,t}}, \sigma_u^2 \sim \mathrm{N}\left(s_{\lambda_{i,t}}, \sigma_u^2 I\right).$$

Subsequently, the conditional distributions of the observed locations are expressed as follows,

$$y_{i,t}|s_{\lambda_{i,t}}, \sigma_u^2, c_t, \theta_t \sim \mathrm{N}\left(\mu_t + (1 + c_t)\, R\,(\theta_t)\left(s_{\lambda_{i,t}} - \mu_t\right), \sigma_u^2\,(1 + c_t)^2\, R\,(\theta_t)\, R^T\,(\theta_t)\right). \tag{4}$$

We note that reliable inference from our model depends on a small σ_u^2 relative to the amount of distortion due to scaling and rotation, and we return to this concept in Sect. 3.1. Based on the latent identities, the data model in (4) allows us to minimize the Procrustes distance (Dryden and Mardia 1998) between configurations of points in the overlapping regions, and the process model that we describe in what follows enables inference about the latent identities.

2.2. PROCESS MODEL

We adopt a parameter expanded data augmentation approach (Royle 2009; Royle and Dorazio 2012) and assume there is a super-population of size M much greater than the total number of observations in a study domain, $\mathcal{D}$, that contains the union of all image footprints. Each individual in the super-population has a binary variable, z_m, representing whether the individual belongs to the population being sampled, where $z_m \sim \text{Bern}(\psi)$ for $m = 1, \ldots, M$. Conditional on the latent identities of the observed individuals, the augmented data are a zero-inflated version of the capture history. The prior specification on the zero-inflation parameter, ψ, along with the super-population size, M, implicitly suggests a prior for the unknown population size, N (Royle et al. 2007).

We let λ_t denote the vector of latent identities indexed by m for the observed individuals in image t. A plausible configuration of λ_t must satisfy two conditions: (a) there are no duplicate identities, and (b) any identity in λ_t must be detectable at time t. Otherwise the probability of observing λ_t is zero. Each individual in the super-population is associated with an activity center, s_m. We let the activity centers be uniformly distributed in the study domain *a priori*. We require that an individual is detectable at time t if and only if it is a member of the population being sampled ($z_m = 1$) and its realized location is inside the image footprint at time t ($u_{m,t} \in \mathcal{F}_t$). In the spatial capture-recapture model by Royle and Young (2008), realized locations are fully augmented for all individuals in the super-population and unobserved $u_{m,t}$ are treated as missing data (the model does not account for measurement error so the observations are the realized locations). However, when the observed individuals are unidentified, accounting for missingness becomes challenging. Therefore, we integrate $u_{m,t}$ from the process model by letting $p_{m,t}$ denote the probability that $u_{m,t}$ falls in $\mathcal{F}_t$ conditional on $\mathcal{F}_t$, the activity center s_m, and the movement process variance σ_u^2, such that

$$p_{m,t} = \mathbb{P}\left(u_{m,t} \in \mathcal{F}_t \middle| \mathcal{F}_t, s_m, \sigma_u^2\right) = \int_{\mathcal{F}_t} \frac{1}{2\pi\sigma_u^2} \exp\left(-\frac{(u - s_m)^{'}(u - s_m)}{2\sigma_u^2}\right) du. \quad (5)$$

Let p_0 denote the baseline detection probability (e.g., sea otter detectability due to diving behaviors). Then we have

$$\mathbb{P}\left(\lambda_{i,t} = m \middle| z_m, s_m, \mathcal{F}_t, \sigma_u^2, p_0\right) = \begin{cases} p_0 \times p_{m,t}, & \text{if } z_m = 1; \\ 0, & \text{otherwise.} \end{cases}$$

Assuming the individuals are independently detected, the probability of observing λ_t is as follows,

$$\mathbb{P}\left(\lambda_t \Big| \{z_m\}_{m=1}^M, \{s_m\}_{m=1}^M, \sigma_u^2, \mathcal{F}_t, p_0\right) = \frac{1}{n_t!} \prod_{m:z_m=1} \left\{ p_0 p_{m,t} \mathbb{I}\left(m \in \lambda_t\right) + \left(1 - p_0 p_{m,t}\right) \mathbb{I}\left(m \notin \lambda_t\right) \right\},$$

(6)

where the factor of $\frac{1}{n_t!}$ indicates that all permutations of λ_t are equally likely *a priori*. The process model induces regularization on the number of unique latent identities by controlling the number of activity centers in an image that belong to the population being sampled. When the super-population is much larger than the total number of observed individuals, under-linkage is likely when each observation seeks its own activity center. However, to infer that a pair of observations in the overlapping region corresponds to different activity centers is to infer that each individual is detected once between two consecutive visits. Such inference, along with any extra activity center in the image that remain undetected, will be penalized by a high detection probability in the model for $\lambda_{i,t}$. The process model thereby motivates linkage between observed locations that are spatially proximal.

2.3. PARAMETER MODEL

We used an informative inverse-gamma prior for σ_u^2 because we have specific knowledge about the extent of sea otter movement that is physically possible between consecutive images (Williams 1989). We imposed a penalization on the second derivatives of the fitted B-splines through the prior variances of α and β. The penalty parameters were selected by cross-validation (Wahba 1978; Wood et al. 2016). We specified $\psi \sim \text{Beta}(0.001, 1)$ to approximate a scale prior for N ($[N] \propto 1/N$, Link, 2013), and we centered the prior for p_0 at 0.75 based on a prior data analysis and as suggested in past studies (Williams et al. 2017; Lu et al. 2019). A full description of prior distributions can be found in Appendix A.

The joint posterior distribution associated with our model is

$$\left[\{\lambda_t\}_{t=1}^T, \{s_m\}_{m=1}^M, \sigma_u^2, \alpha, \beta, \{z_m\}_{m=1}^M, p_0, \psi \Big| Y\right] \propto \prod_{t=1}^T \prod_{i=1}^{n_t} \left[y_{i,t} \Big| s_{\lambda_{i,t}}, \sigma_u^2, \alpha, \beta \right] \times \prod_{m=1}^M [s_m]$$

$$\times \prod_{t=1}^T \left[\lambda_t \Big| \{z_m\}_{m=1}^M, \{s_m\}_{m=1}^M, \sigma_u^2, \alpha, \beta, p_0 \right] \times [p_0]$$

$$\times \prod_{m=1}^M [z_m|\psi] \times [\psi] \times \left[\sigma_u^2\right] \times [\alpha] \times [\beta].$$

The distortion parameters, c_t and θ_t, in Eq. 4 and the image footprint, $\mathcal{F}_t$, in Eq. 6 are deterministic functions of α and β, and are therefore replaced by the basis function coefficients in the above expression. We implemented our model using MCMC and provide a full description of the algorithm in Supplementary Appendix A.

3. APPLICATION

3.1. SIMULATION

We simulated a population of $N = 200$ individuals and sampled their activity centers s_m, for $m = 1, \ldots, N$, uniformly from a 100 m × 2000 m study domain, $\mathcal{D}$, to emulate the population intensity in the case study. For $t = 1, \ldots, T$, $T = 50$, we sampled realized locations $\boldsymbol{u}_{m,t} \sim \text{N}\left(s_m, \sigma_u^2 \boldsymbol{I}\right)$. We let σ_u^2 be 0.25 based on the estimated maximum underwater speed of sea otters according to empirical studies (Williams 1989). For the measurement process, we set the image centers to be equally spaced between $\boldsymbol{\mu}_1 = (50, 50)'$ and $\boldsymbol{\mu}_{50} = (1950, 50)'$ and let the footprint template at time t, $\mathcal{Q}_t$, be a 58 m × 58 m square centered at $\boldsymbol{\mu}_t$ and parallel to the horizontal axis. We generated distortion parameters from cubic B-splines with coefficients $\boldsymbol{\alpha} = \boldsymbol{\beta} = (0.1, 0.2, 0.1, -0.1, -0.2)'$ and obtained the image footprint $\mathcal{F}_t$ using Eq. 3. When $\boldsymbol{u}_{m,t} \in \mathcal{F}_t$, we detect individual m at time t with probability $p_0 = 0.75$ as informed by past studies (Williams et al. 2017; Lu et al. 2019). We recorded the distorted locations of the detected individuals by Eq. 1. Figure 1 illustrates the simulated image footprints and the true locations as well as the corresponding footprint templates and the observed locations.

In our implementation of the model, we let the super-population be of size $M = 3000$. We ran the MCMC algorithm in R version 3.0.2 (R Core Team 2019) for 15,000 iterations. Our algorithm took 2.5 hours on a 2.5 GHz Intel Core i5 processor. Advanced sampling strategies like the split-merge Metropolis-Hastings updates on the latent identities can be used to expedite computation (Jain and Neal 2004), and parallel computing techniques like recursive Bayesian methods can improve statistical scalability in future implementations (Hooten et al. 2021). We used a burn-in of 5000 iterations and obtained posterior realizations of population size as a derived quantity from the remaining $K = 10000$ posterior samples of z_m as

$$N^{(k)} = \sum_{m=1}^{M} z_m^{(k)}, \ k = 1, \ldots, K. \tag{7}$$

We obtained posterior realizations of the number of unique individuals from all observations by counting unique labels in the posterior samples of $\{\lambda_t\}_{t=1}^{T}$ as

$$N_0^{(k)} = \left| \left\{ \lambda_t^{(k)} \right\}_{t=1}^{T} \right|, \ k = 1, \ldots, K. \tag{8}$$

Our model captured the true parameters within their respective 95% credible intervals, which we summarize in Supplementary Table 1.

Two recent studies have used aerial photographs to estimate sea otter abundance in Glacier Bay, Alaska. Lu et al. (2019) proposed a nonlinear reaction-diffusion process model for population intensity, but used only every other image in accordance with the assumptions of their model. An arbitrary selection of images to use for data analysis may lead to bias in abundance estimation, especially if population intensity is spatially heterogeneous. Although our method is not directly comparable to that of Lu et al. (2019), we can compare the
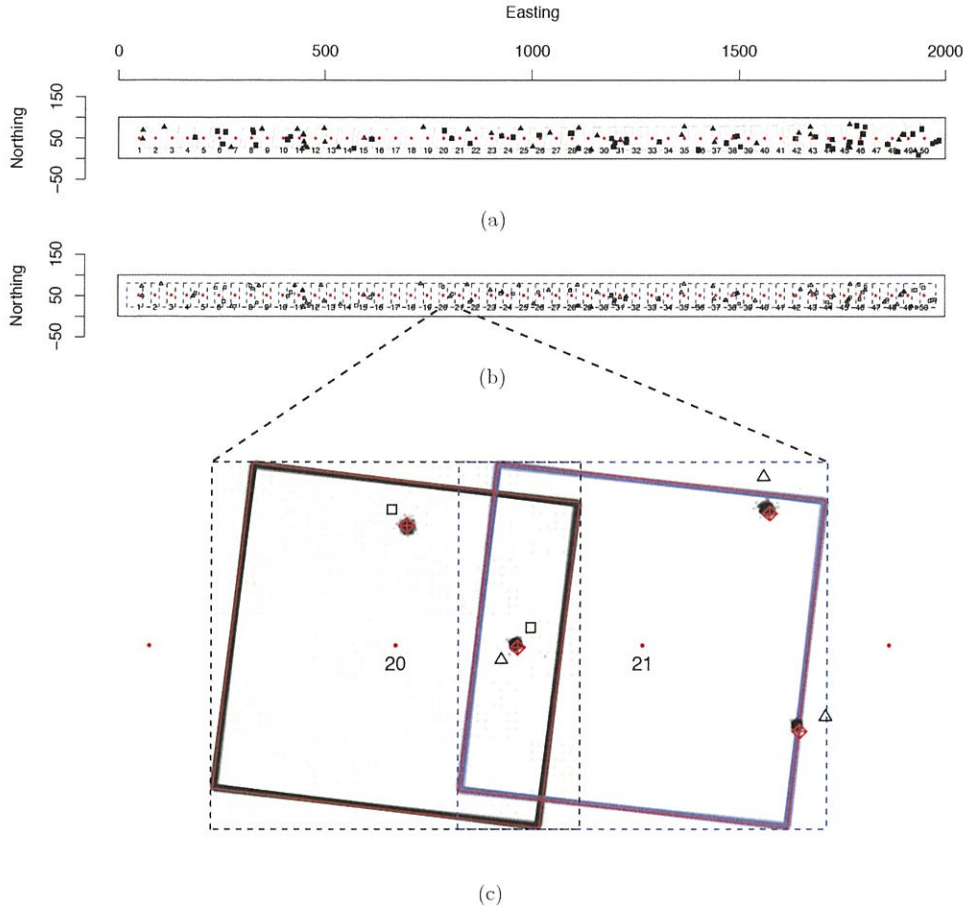
Figure 1.   **a** Simulated image footprints, $\mathcal{F}_t$, overlaid with true locations, $\boldsymbol{u}_{i,t}$. The time-indexed points represent image centers, $\boldsymbol{\mu}_t$. True locations are marked with "■" in even images and "▲" in odd images. The largest rectangle containing all images is the study domain, $\mathcal{D}$; **b** simulated footprint templates (dashed rectangles), $\mathcal{Q}_t$, overlaid with observed locations, $\boldsymbol{y}_{i,t}$, that are marked with "□" in even images and "△" in odd images; **c** a focused illustration on observed images 20 and 21 (dashed rectangles), overlaid with posterior samples of image footprints (solid rectangles) and activity centers (points) with their truths (crossed diamonds) .

estimated number of unique individuals in all images because it refers to the observed abundance. We observed 111 locations from all images in the above simulation, which correspond to 90 unique individuals in truth. Our model estimated a posterior mean of 90 unique individuals. However, the number of unique individuals from counting all the odd images is 60, and the number of unique individuals from counting all the even images is 51. Discarding half of the images led to inconsistent and insufficient counts, whereas we improved abundance estimates by accounting for duplicate individuals in overlapping regions.

Williams et al. (2017) proposed an N-mixture model where the counts from overlapping images are considered temporal replicates. The model divides images into mutually exclusive regions of overlaps and non-overlaps and denotes $y(A_i, j)$ as the count from the jth overlap of region A_i, such that $\cup_{i=1}^n A_i = \cup_{t=1}^T \mathcal{F}_t$ and $A_i \cap A_j = \emptyset$, $i \neq j$. Under the
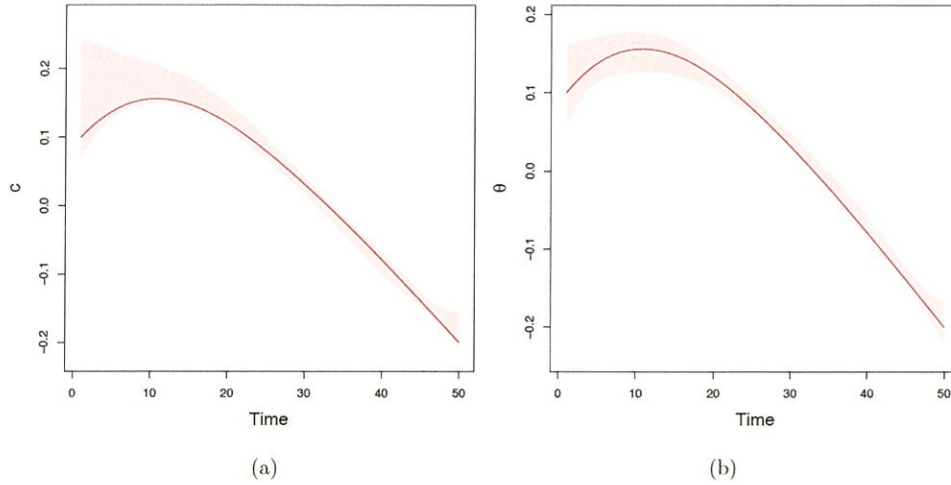
Figure 2. **a** Estimated point-wise 95% credible interval overlaid with the truth for the scaling parameter, c; **b** estimated point-wise 95% credible interval overlaid with the truth for the rotation parameter, θ .

assumption of homogeneous detection probability p_0 and population intensity η, the counts are modeled by

$$y\left(A_i, j\right) \sim \text{Binom}\left(N\left(A_i\right), p_0\right)$$
$$N\left(A_i\right) \sim \text{Pois}\left(\eta|A_i|\right),$$

$$(9)$$

where $|A_i|$ is the area of A_i. Although Williams et al. (2017) accounted for heterogeneity in p_0 and η based on spatial covariates, we fit the homogeneous version of their model in Eq. 9 to our simulated data using an MCMC algorithm. A posterior realization of population size is obtained as a derived quantity by $N^{(k)} = \eta^{(k)}|\mathcal{D}|$, for $k = 1, \ldots, K$ MCMC iterations. The estimated posterior mean abundance was 178 with a 95% credible interval (142, 216). Both the method by Williams et al. (2017) and our method were able to recover the true population abundance in simulation; nonetheless, our process model distinguished sea otter detectability due to diving from that due to temporary emigration from the image footprints (Kendall et al. 1997). In addition to abundance estimation, our estimated activity centers can be used to inform spatial heterogeneity of the population intensity and our estimated distortion parameters can be used to reconstruct the aircraft trajectory via trigonometric projections.

To evaluate our model performance in linkage estimation, we used false discovery rate (FDR) and false negative rate (FNR) as recommended by Steorts (2015) to account for the large number of non-links in our application. There are four possible results when comparing the estimated linkage and the truth:

1. True positive (TP): two individuals have the same latent identity in both the estimation and the truth;

2. False positive (FP): two individuals are estimated to have the same latent identity when they are actually different;

Table 1. True parameter values and marginal posterior means (95% credible intervals) for population size (N) and the number of unique individuals (N_0) under different simulated movement uncertainties (σ_u^2)

σ_u^2	N	Posterior mean (95% CI)	N_0	Posterior mean (95% CI)
0.25	200	192 (160, 233)	91	90 (90, 91)
1	200	191 (155, 241)	87	88 (87, 91)
2.5	200	251 (196, 327)	91	95 (93, 97)
10	200	364 (216, 668)	88	100 (93, 108)

3. True negative (TN): two individuals have different latent identities in both the estimation and the truth;

4. False negative (FN): two individuals are estimated to have different latent identities when they are actually the same.

We computed the posterior mean FDR and FNR as $\mathbb{E}[\text{FDR}|Y] = \frac{1}{K}\sum_{k=1}^{K}\frac{\text{FP}^{(k)}}{\text{FP}^{(k)}+\text{TP}^{(k)}} = 0.000001$ and $\mathbb{E}[\text{FNR}|Y] = \frac{1}{K}\sum_{k=1}^{K}\frac{\text{FN}^{(k)}}{\text{FN}^{(k)}+\text{TP}^{(k)}} = 0.001$ based on the model fit to the simulated data.

Posterior realizations of the scaling and rotation parameters, c and θ, were obtained as derived quantities using Eq. 2, and posterior realizations of the image footprints, $\mathcal{F}_t$, were obtained as derived quantities using Eq. 3. Figure 1 illustrates posterior samples of the image footprints and the activity centers overlaid with their truth for a subset of images (images 20 and 21). Our model performed well, linking observations that correspond to the same individual in the overlapping region and correctly estimating their activity centers despite distortion. Figure 2 demonstrates the point-wise 95% credible intervals for c and θ. The point-wise 95% credible intervals contained the true simulated values for both parameters.

Lastly, we demonstrate our model inference using simulated data with increasing levels of individual movement, σ_u^2, while the other parameters are held constant. We note that any σ_u^2 significantly larger than 0.25 would be unrealistic for sea otters in southeastern Alaska; nonetheless, the following demonstration serves to emphasize a viable condition for applying our method in other survey scenarios. Table 1 summarizes the posterior distributions of the number of unique individuals and population size along with their truth under different values of σ_u^2. The true numbers of unique individuals vary between simulations due to dependence on σ_u^2. The estimated 95% credible interval for N_0 widens as individual movement increases, indicating less certainty in the linkage process. Consequently, the estimated 95% credible interval for N expands along with σ_u^2, and the credible intervals when $\sigma_u^2 = 10$ did not contain the respective truths for N_0 or N.

3.2. CASE STUDY

Sea otter populations have undergone significant fluctuations throughout their range over the past two centuries (Jameson et al. 1982). After being hunted to near extinction during the maritime fur trade, sea otter populations have recovered in many areas due to a combination of conservation efforts, translocations, and environmental changes (Larson

Table 2.   Marginal posterior means and 95% credible intervals for the case study

Parameter	Posterior mean (95% CI)
p_0	0.64 (0.52, 0.75)
ψ	0.19 (0.15, 0.24)
N	566 (453, 704)
σ_u^2	0.45 (0.34, 0.59)

et al. 2014; Eisaguirre et al. 2021). Monitoring sea otter colonization in Glacier Bay provides important insight into the ability of a keystone species to recover from near extirpation and to understand their role in structuring the nearshore food web in Glacier Bay (Williams et al. 2019). From 1993 to 2012, observer-based aerial surveys were conducted from small single-engine aircraft along systematic transects (Esslinger et al. 2015). Beginning in 2017, aerial photographic methods (Womble et al. 2018) were conducted using model-based optimized surveys (Williams et al. 2019). Aerial photographic images were post-processed by trained observers that counted the number of sea otters in each image. For our case study, we analyzed a sequence of 20 consecutive images with a total of 151 observations (see Fig. 3 in Supplementary Material for an example of real images). Sea otter locations were recorded for 60 m × 90 m footprint templates with their long sides perpendicular to the direction of aircraft movement (vectors connecting consecutive image centers). Figure 3 illustrates the observed locations overlaid with footprint templates. Our study domain was a 300 m × 1000 m rectangular region containing all image footprints as shown in Fig. 3.

We let the super-population be of size $M = 3000$ and ran the MCMC algorithm for 15000 iterations with a burn-in of 5000 iterations. Table 2 summarizes the marginal posterior distributions from the case study. Our estimated detection probability agrees with the estimates from previous studies (Williams et al. 2017; Lu et al. 2019). Posterior realizations of population size were obtained as derived quantities by Eq. 7.

Our model inferred a posterior mean of 125 unique individuals among the 151 observations using Eq. 8. We illustrate posterior samples of the image footprints, $\mathcal{F}_t$, obtained as derived quantities using Eq. 3 and posterior samples of the true locations, $\boldsymbol{u}_{i,t}$, obtained as derived quantities using Eq. 1 for a subset of images ($t = 8, 9$) in Fig. 3. Using our model, we estimated counterclockwise rotation as the distortion process for both images, thereby linking the two pairs of observations in the overlapping region. The posterior mean linkage probability was 0.98 for observation pairs (a, h) and (b, i), and all other observation pairs have less than 0.02 posterior mean linkage probabilities. Figure 4 demonstrates the point-wise 95% credible intervals overlaid with the posterior means for scaling and rotation, respectively.

4. DISCUSSION

We presented a novel method to perform entity resolution and population size estimation using individual locations obtained from aerial imagery data of sea otters. We coupled

(a)

(b)
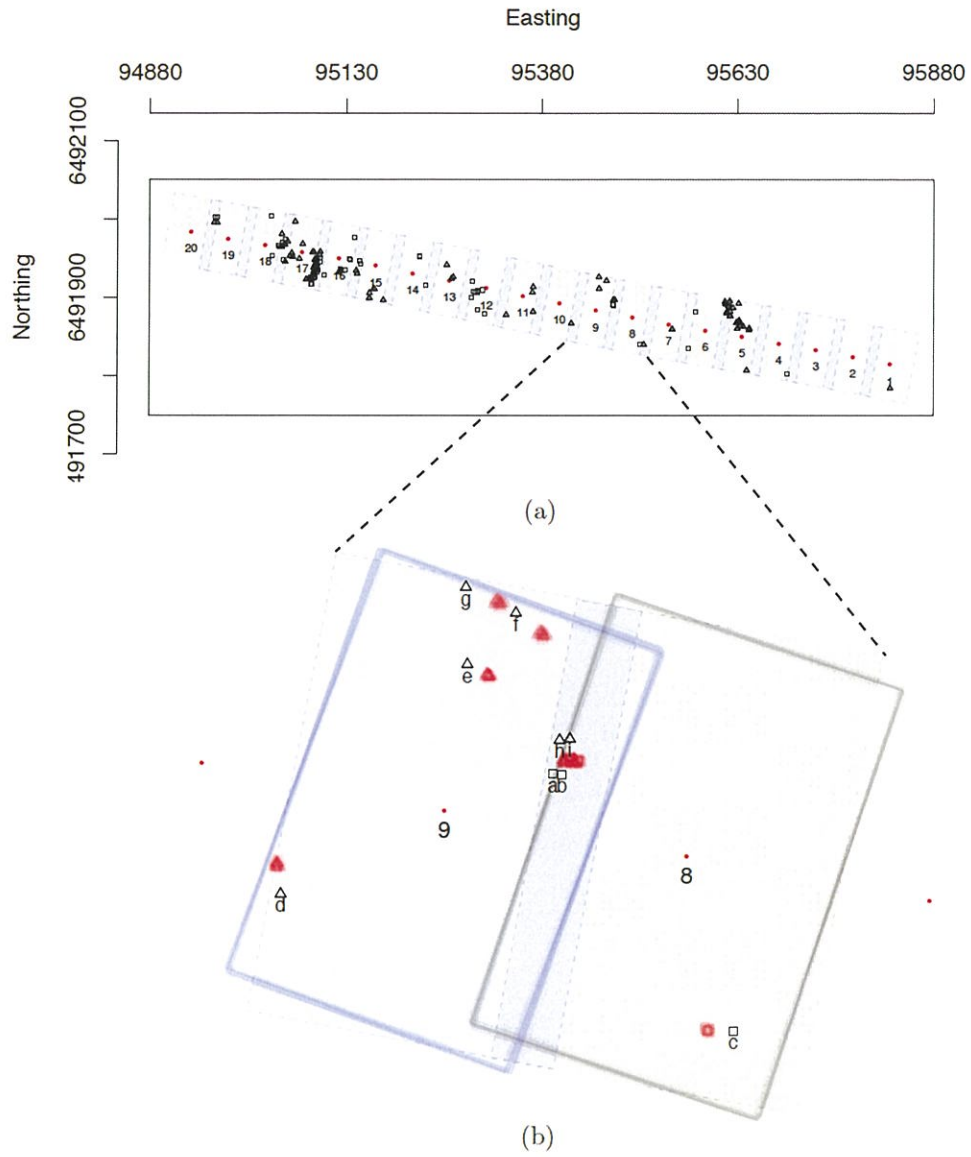
Figure 3. **a** Observations from the case study. Footprint templates (dashed rectangles), $\mathcal{Q}_t$, are overlaid with observed locations, $y_{i,t}$, that are marked with "□" in even images and "△" in odd images. The time-indexed points represent image centers, μ_t. The largest rectangle containing all templates is the study domain, $\mathcal{D}$; **b** a focused illustration on observed images 8 and 9 (dashed rectangles), overlaid with posterior samples of image footprints (solid rectangles), $\mathcal{F}_t$. Observed locations are indexed by letters, and posterior samples of true locations, $u_{i,t}$, are shown in solid squares in image 8 and solid triangles in image 9.

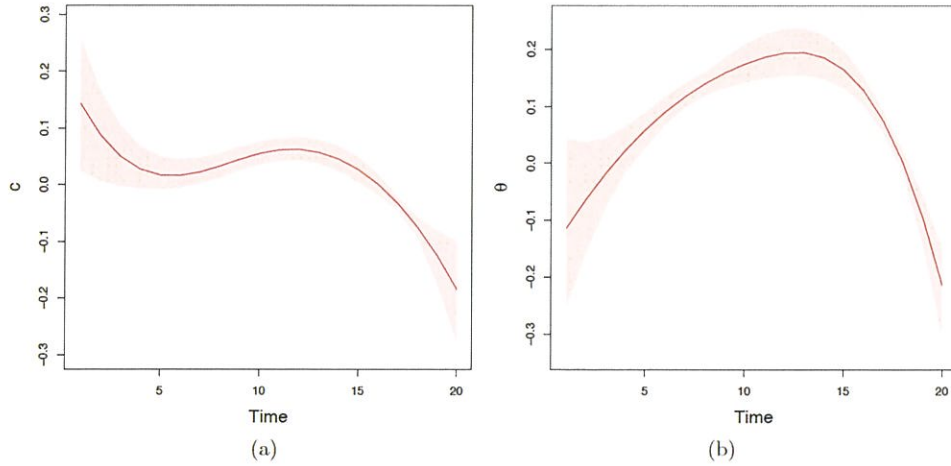Figure 4.   **a** Estimated posterior mean and point-wise 95% credible interval for the scaling parameter, c; **b** estimated posterior mean and point-wise 95% credible interval for the rotation parameter, θ .

record linkage and capture-recapture models to accommodate important features of aerial imagery data. Our unified framework allows information exchange and uncertainty propagation between the estimation of linkage structure and population abundance, and our model is adequate for both inferential tasks.

Record linkage models are often sensitive to parameters that control linkage probability. In a sensitivity analysis for the graphical record linkage model, Steorts (2015) showed that linkage inference is only reliable when a very precise prior is used on the parameter for distortion probability. In the Bayesian alignment model, Green and Mardia (2005) advised that informative priors be used for parameters that dictate matching tendency. In our model, linkage of observed locations is motivated by their proximity in Euclidean distance to latent activity centers. Therefore, as expected, our model is sensitive to σ_u^2, the parameter controlling movement. Reliable inference requires that animal movement between consecutive detections be small relative to distortion, otherwise the model would struggle to identify unique individuals using locations only. Fortunately, much is known about movement characteristics of many species and this information can be used to specify an informative prior for σ_u^2. During aerial surveys in Glacier Bay, Alaska, the time lapse between consecutive images is so brief (1 second) that sea otter movement is significantly limited by their physical capability, thus we specified the prior for σ_u^2 such that movement distance between consecutive images was less than a meter (Williams 1989). We provide details for a sensitivity analysis of prior distributions on σ_u^2 in Supplementary Appendix B. In addition to limited individual movement, our method could potentially benefit from more overlapping regions and higher population intensities because they provide more instances for linkage. On the other hand, our method may be hindered by extensive distortions in the image footprints or highly clustered populations where distances between the true activity centers are closer than σ_u.

Although our method is designed to link observed individuals and estimate population size simultaneously, it can be useful even when the objective is only one of the two. The

output of a record linkage model provides insight about the number of unique individuals observed at least once, and abundance estimation requires only the additional subset of population that is not observed. Population models can be used to provide prior information about the total number of latent individuals in a graphical record linkage model (Tancredi et al. 2018), a parameter that has also proven to be influential for inference (Steorts 2015). Detection mechanisms can guide learning about the number of times an individual's record is observed: High detection probabilities indicate frequent observations of an individual, thereby promoting linkage; low detection probabilities indicate few observations of the individual, thereby proposing new latent identities. Our model assumptions can be generalized to account for more complicated monitoring situations. For example, hypergeometric models may be used in place of binomial models in capture-recapture studies when individual detections are correlated due to sampling without replacement from a finite population (Darroch 1958; Link et al. 2009; Tancredi and Liseo 2011). We may also model heterogeneity in p_0 to account for factors such as animal diving in response to aircraft disturbance and survey conditions that affect the backdrop (e.g., kelp, sun angle, sea state).

The use of observed locations in our model helped us better understand the spatial heterogeneity in population intensity. Under a uniform prior on s_m, the variation in population intensity is implicitly reflected through the estimated activity centers. A natural extension to our method is to model the spatial distribution of activity centers explicitly (Efford 2004, 2011; Brost et al. 2017, 2020). We could account for heterogeneity in the distribution of activity centers using a species distribution model (SDM; e.g., Hefley and Hooten, 2016). An SDM is often specified as a spatial point process model, which, in our case, could take the form

$$[s_m | x(s_m)] = \frac{\exp\left(x(s_m)' \beta\right)}{\int_{\mathcal{D}} \exp(x(s)'\beta)\, ds},$$

for $m = 1, \ldots, M$, where $x(s_m)$ denotes the vector of spatial covariates at s_m and β denotes the associated coefficients. Alternatively, we could attribute heterogeneity in the distribution of activity centers to the interaction among individuals which could be modeled mechanistically (e.g., Scharf et al., 2016).

Although our model was designed for aerial imagery data from sea otter population surveys in Glacier Bay, Alaska, our framework can be adapted for a variety of applications that involve intersecting fields of observation (Borchers et al. 2020). Our method is also useful for aligning unlabeled point patterns with consistent measurement error, such as reconstruction of a three-dimensional object from two-dimensional views (Ourselin et al. 2001; Rezende et al. 2016) and reconstruction of a movement trajectory using multiple snapshots (Ando 1991; Du et al. 2016).

ACKNOWLEDGEMENTS

APPENDIX A: PRIOR DISTRIBUTIONS

$$p_0 \sim \text{Beta}(3, 1),$$
$$\psi \sim \text{Beta}(0.001, 1),$$
$$\sigma_u^2 \sim \text{IG}(100, 25),$$
$$s_m \sim \text{Unif}(\mathcal{D}), \quad m = 1, \ldots, M,$$
$$\alpha \sim \text{N}(0, 0.001R + 0.01I),$$
$$\beta \sim \text{N}(0, 0.001R + 0.01I),$$

where $R = \left(D_2^-\right)' D_2$ and $D_2 = \begin{bmatrix} 1 & -2 & 1 & 0 & 0 \\ 0 & 1 & -2 & 1 & 0 \\ 0 & 0 & 1 & -2 & 1 \end{bmatrix}$.

REFERENCES

Anderson M, Fienberg SE (1999) Who counts? The politics of census-taking in contemporary America. Russell Sage Foundation

Ando H (1991) Dynamic reconstruction of 3d structure and 3d motion. In: Proceedings of the IEEE workshop on visual motion, pp 101–102

Barker RJ, Schofield MR, Link WA, Sauer JR (2018) On the reliability of N-mixture models for count data. Biometrics 74:369–377

Betancourt B, Zanella G, Miller JW, Wallach H, Zaidi A, Steorts RC (2016) Flexible models for microclustering with application to entity resolution. In Advances in neural information processing systems, pp 1417–1425

Borchers DL, Nightingale P, Stevenson BC, Fewster RM (2020) A latent capture history model for digital aerial surveys. Biometrics

Brost BM, Hooten MB, Small RJ (2017) Leveraging constraints and biotelemetry data to pinpoint repetitively used spatial features. Ecology 98(1):12–20

Brost BM, Hooten MB, Small RJ (2020) Model-based clustering reveals patterns in central place use of a marine top predator. Ecosphere 11:e03123

Brown M, Lowe DG (2015) Automatic panoramic image stitching using invariant features. Int J Comput Vision 74:59–73

Buckland ST, Burt ML, Rexstad EA, Mellor M, Williams AE, Woodward R (2012) Aerial surveys of seabirds: the advent of digital methods. J Appl Ecol 49:960–967

Caughley G (1974) Bias in aerial survey. J Wildl Manag 38(4):921–933

Christen P (2011) A survey of indexing techniques for scalable record linkage and deduplication. IEEE Trans Knowl Data Eng 24:1537–1555

Copas J, Hilton F (1990) Record linkage: statistical models for matching computer records. J R Stat Soc A Stat Soc 153:287–312

Darroch JN (1958) The multiple capture census i. Estimation of a closed population. Biometrika 45:343–358

Dennis EB, Morgan BJT, Ridout MS (2015) Computational aspects of N-mixture models. Biometrics 71:237–246

Dryden IL, Mardia KV (1998) Statistical analysis of shape. Wiley

Du Y, Wong Y, Liu Y, Han F, Gui Y, Wang Z, Kankanhalli M, Geng W (2016) Marker-less 3d human motion capture with monocular image sequence and height-maps. In: European conference on computer vision. Springer, pp 20–36

Efford M (2004) Density estimation in live-trapping studies. Oikos 106:598–610

Efford MG (2011) Estimation of population density by spatially explicit capture-recapture analysis of data from area searches. Ecology 92:2202–2207

Eisaguirre JM, Williams PJ, Lu X, Kissling ML, Beatty WS, Esslinger GG, Womble JN, Hooten MB (2021) Diffusion modeling reveals effects of multiple release sites and human activity on a recolonizing apex predator. Mov Ecol 9:34

Esslinger GG, Esler D, Howlin S, Starcevich L (2015) Monitoring population status of sea otters (Enhydra lutris) in Glacier Bay National Park and Preserve, Alaska: options and considerations. US Department of the Interior, US Geological Survey

Fellegi IP, Sunter AB (1969) A theory for record linkage. J Am Stat Assoc 64:1183–1210

Fortini M, Liseo B, Nuccitelli A, Scanu M (2001) On Bayesian record linkage. Res Official Stat 4:185–198

Green PJ, Mardia K (2005) Bayesian alignment using hierarchical models, with application in protein bioinformatics. Biometrika 93(2):235–254

Gross JW, Heumann BW (2016) A statistical examination of image stitching software packages for use with unmanned aerial systems. Photogr Eng Remote Sens 82(6):419–425

Hefley TJ, Broms KM, Brost BM, Buderman FE, Kay SL, Scharf HR, Tipton JR, Williams PJ, Hooten MB (2017) The basis function approach to modeling autocorrelation in ecological data. Ecology 98:632–646

Hefley TJ, Hooten MB (2016) Hierarchical species distribution models. Curr Lands Ecol Rep 1:87–97

Hooten MB, Johnson DS, Brost BM (2021) Making recursive Bayesian inference accessible. Am Stat 75:185–194

Jain S, Neal RM (2004) A split-merge Markov chain Monte Carlo procedure for the Dirichlet process mixture model. J Comput Graph Stat 13:158–182

Jameson RJ, Kenyon KW, Johnson AM, Wight HM (1982) History and status of translocated sea otter populations in North America. Wildl Soc Bull 10(2):100–107

Jaro MA (1989) Advances in record-linkage methodology as applied to matching the 1985 census of Tampa, Florida. J Am Stat Assoc 84:414–420

Kendall WL, Nichols JD, Hines JE (1997) Estimating temporary emigration using capture-recapture data with Pollock's robust design. Ecology 78:563–578

Ketz AC, Johnson TL, Hooten MB, Hobbs NT (2019) A hierarchical Bayesian approach for handling missing classification data. Ecol Evol 9(6):3130–3140

LaPorte RE, McCarty D, Bruno G, Tajima N, Baba S (1993) Counting diabetes in the next millennium: application of capture-recapture technology. Diabetes Care 16:528–534

Larsen MD (2004) Record linkage using finite mixture models. An essential journey with donald Rubin's statistical family, applied Bayesian modeling and causal inference from incomplete-data perspectives, pp 309–318

Larsen MD, Rubin DB (2001) Iterative automated record linkage using mixture models. J Am Stat Assoc 96:32–41

Larson SE, Bodkin JL, VanBlaricom GR (2014) Sea Otter conservation. Academic Press

Levin A, Zomet A, Peleg S, Weiss Y (2004) Seamless image stitching in the gradient domain. In: European conference on computer vision. Springer, pp 377–389

Link WA (2013) A cautionary note on the discrete uniform prior for the binomial N. Ecology 94(10):2173–2179

Link WA, Yoshizaki J, Bailey LL, Pollock KH (2009) Uncovering a latent multinomial: analysis of mark-recapture data with misidentification. Biometrics 66:178–185

Liseo B, Tancredi A (2011) Bayesian estimation of population size via linkage of multivariate normal data sets. J Official Stat 27:491

Lu X, Williams PJ, Hooten MB, Powell JA, Womble JN, Bower MR (2019) Nonlinear reaction-diffusion process models improve inference for population dynamics. Environmetrics 31(3):e2604

Lum K, Price ME, Banks D (2013) Applications of multiple systems estimation in human rights research. Am Stat 67:191–200

McGlincy MH (2004) A Bayesian record linkage methodology for multiple imputation of missing links. In: ASA proceedings of the joint statistical meetings. American Statistical Association, Alexandria, VA, pp 4001–4008

Ourselin S, Roche A, Subsol G, Pennec X, Ayache N (2001) Reconstructing a 3D structure from serial histological sections. Image Vis Comput 19:25–31

R Core Team (2019) R: A language and environment for statistical computing. R Foundation for Statistical Computing, Vienna, Austria

Rezende DJ, Eslami SA, Mohamed S, Battaglia P, Jaderberg M, Heess N (2016) Unsupervised learning of 3d structure from images. In: Advances in neural information processing systems, pp 4996–5004

Royle JA (2009) Analysis of capture-recapture models with individual covariates using data augmentation. Biometrics 65:267–274

Royle JA, Dorazio R (2012) Parameter-expanded data augmentation for Bayesian analysis of capture-recapture models. J Ornithol 152:521–537

Royle JA, Dorazio RM, Link WA (2007) Analysis of multinomial models with unknown index using data augmentation. J Comput Graph Stat 16:67–85

Royle JA, Young KV (2008) A hierarchical model for spatial capture-recapture data. Ecology 89(8):2281–2289

Sadinle M (2018) Bayesian propagation of record linkage uncertainty into population size estimation of human rights violations. Ann Appl Stat 12(2):1013–1038

Scharf HR, Hooten MB, Fosdick BK, Johnson DS, London JM, Durban JW et al (2016) Dynamic social networks based on movement. Ann Appl Stat 10:2182–2202

Steorts RC (2015) Entity resolution with empirically motivated priors. Bayesian Anal 10(4):849–875

Steorts RC, Hall R, Fienberg SE (2015) A Bayesian approach to graphical record linkage and deduplication. J Am Stat Assoc 111:1660–1672

Steorts RC, Ventura SL, Sadinle M, Fienberg SE (2014) A comparison of blocking methods for record linkage. International conference on privacy in statistical databases. Springer, Cham, pp 253–268

Szeliski R (2006) Image alignment and stitching: a tutorial. Found Trends® Comput Graph Vis 2:1–104

Tancredi A, Liseo B (2011) A hierarchical Bayesian approach to record linkage and population size problems. Ann Appl Stat 5(2B):1553–1585

Tancredi A, Steorts R, Liseo B et al (2018) A unified framework for de-duplication and population size estimation. Bayesian Anal 15(2):633–682

Ver Hoef JM (2014) Aerial survey data. Statistics Reference Online, Wiley StatsRef

Wahba G (1978) Improper priors, spline smoothing and the problem of guarding against model errors in regression. J Roy Stat Soc Ser B 40(3):364–372

Wallach H, Jensen S, Dicker L, Heller K (2010) An alternative prior process for nonparametric Bayesian clustering. In: Proceedings of the thirteenth international conference on artificial intelligence and statistics, pp 892–899

Williams PJ, Hooten MB, Esslinger GG, Womble JN, Bodkin JL, Bower MR (2019) The rise of an apex predator following deglaciation. Divers Distrib 25:895–908

Williams PJ, Hooten MB, Womble JN, Bower MR (2017) Estimating occupancy and abundance using aerial images with imperfect detection. Methods Ecol Evol 8:1679–1689

Williams PJ, Schroeder C, Jackson P (2020) Estimating reproduction and survival of unmarked juveniles using aerial images and marked adults. J Agric Biol Environ Stat 25:133–147

Williams TM (1989) Swimming by sea otters: adaptations for low energetic cost locomotion. J Comp Physiol A 164(6):815–824

Winkler WE (1995) Matching and record linkage. Bus Surv Methods 1:355–384

Winkler WE (2006) Overview of record linkage and current research directions. In: Bureau of the Census

Womble J, Williams P, Johnson W, Taylor-Thomas L, Bower M (2018) Sea otter monitoring protocol for Glacier Bay National Park, Alaska: Version SO-2017.1. Natural Resource Report NPS/SEAN/NRR—2018/1762, National Park Service, Fort Collins, Colorado

Wood SN, Pya N, Safken B (2016) Smoothing parameter and model selection for general smooth models. J Am Stat Assoc 111(516):1548–1563

Wright JA, Baker RJ, Schofield MR, Frantz AC, Byrom AE, Gleeson DM (2009) Incorporating genotype uncertainty into mark-recapture-type models for estimating abundance using DNA samples. Biometrics 65:833–840

Diffusion modeling reveals effects of multiple release sites and human activity on a recolonizing apex predator

Joseph M. Eisaguirre[1,2]* , Perry J. Williams[1], Xinyi Lu[3], Michelle L. Kissling[2,8], William S. Beatty[2,9], George G. Esslinger[4], Jamie N. Womble[5,6] and Mevin B. Hooten[3,7]

Abstract

Background: Reintroducing predators is a promising conservation tool to help remedy human-caused ecosystem changes. However, the growth and spread of a reintroduced population is a spatiotemporal process that is driven by a suite of factors, such as habitat change, human activity, and prey availability. Sea otters (*Enhydra lutris*) are apex predators of nearshore marine ecosystems that had declined nearly to extinction across much of their range by the early 20th century. In Southeast Alaska, which is comprised of a diverse matrix of nearshore habitat and managed areas, reintroduction of 413 individuals in the late 1960s initiated the growth and spread of a population that now exceeds 25,000.

Methods: Periodic aerial surveys in the region provide a time series of spatially-explicit data to investigate factors influencing this successful and ongoing recovery. We integrated an ecological diffusion model that accounted for spatially-variable motility and density-dependent population growth, as well as multiple population epicenters, into a Bayesian hierarchical framework to help understand the factors influencing the success of this recovery.

Results: Our results indicated that sea otters exhibited higher residence time as well as greater equilibrium abundance in Glacier Bay, a protected area, and in areas where there is limited or no commercial fishing. Asymptotic spread rates suggested sea otters colonized Southeast Alaska at rates of 1–8 km/yr with lower rates occurring in areas correlated with higher residence time, which primarily included areas near shore and closed to commercial fishing. Further, we found that the intrinsic growth rate of sea otters may be higher than previous estimates suggested.

Conclusions: This study shows how predator recolonization can occur from multiple population epicenters. Additionally, our results suggest spatial heterogeneity in the physical environment as well as human activity and management can influence recolonization processes, both in terms of movement (or motility) and density dependence.

Keywords: Bayesian, Biological invasion, Ecological diffusion, Partial differential equation, Reaction-diffusion, Reintroduction, Sea otter

---

*Correspondence: joseph_eisaguirre@fws.gov
[1]Department of Natural Resources and Environmental Science, University of Nevada Reno, Reno, NV, USA
[2]United States Fish & Wildlife Service, Marine Mammals Management, Anchorage, AK, USA
Full list of author information is available at the end of the article

Background

The global decline of apex predators has changed ecosystems [1–4]. These changes continue to have cascading effects across trophic levels, resulting in new ecosystem states of varying resilience [2]. When an apex predator is reintroduced, however, such a perturbation followed by continued growth and expansion of the population can change ecological communities and revert an ecosystem to a previous state [5]. Although often controversial, such shifts in ecosystem state can achieve conservation goals and afford ecological and economic benefits [6].

Predator reintroductions are sometimes proposed to recover ecosystem services or remedy human-caused declines, such as those due to overharvest [6, 7]. One of the most successful and celebrated efforts has been the reintroduction of wolves (*Canis lupus*) and subsequent recovery in the Greater Yellowstone Ecosystem. Wolves recolonized the area at a rate of about 10 km per year [8], and their renewed presence mediated over-browsing by elk (*Cervus canadensis*) and allowed the previous vegetation structure to return, subsequently driving additional recovery across the ecosystem [5]. Many reintroductions are unsuccessful, however [9, 10], because the distributions of resources, sources of mortality, and the physical environment—factors that influence recolonization—are highly variable through space and time [11–13]. Recolonization by apex predators is thus spatiotemporally dynamic, especially over large geographic areas that are characterized by finer-scale ecological variability [7]. Therefore, recolonization by a predator, as well as its abundance and persistence, will vary over space and through time.

Sea otters (*Enhydra lutris*), apex predators of nearshore marine systems, were harvested during the commercial fur trade up until the early 20th century, at which point they had declined nearly to extinction across most of their range [14]. For decades following, the nearshore marine ecosystems in many areas transitioned to, and persisted in, alternative states dominated by benthic herbivores that sea otters normally prey upon [15]. Legislation, beginning with the Fur Seal Treaty (1911), followed by the Marine Mammal Protection Act (MMPA; 1972) and the Endangered Species Act (1977), protected sea otters from harvest, with the exception of harvest by Alaska Natives for subsistence and handicraft, per the MMPA [14]. This protection facilitated sea otter population growth and expansion across parts of their range, which has been reverting the nearshore ecosystem in some of these areas to the historical predator-dominated state [6, 15–17].
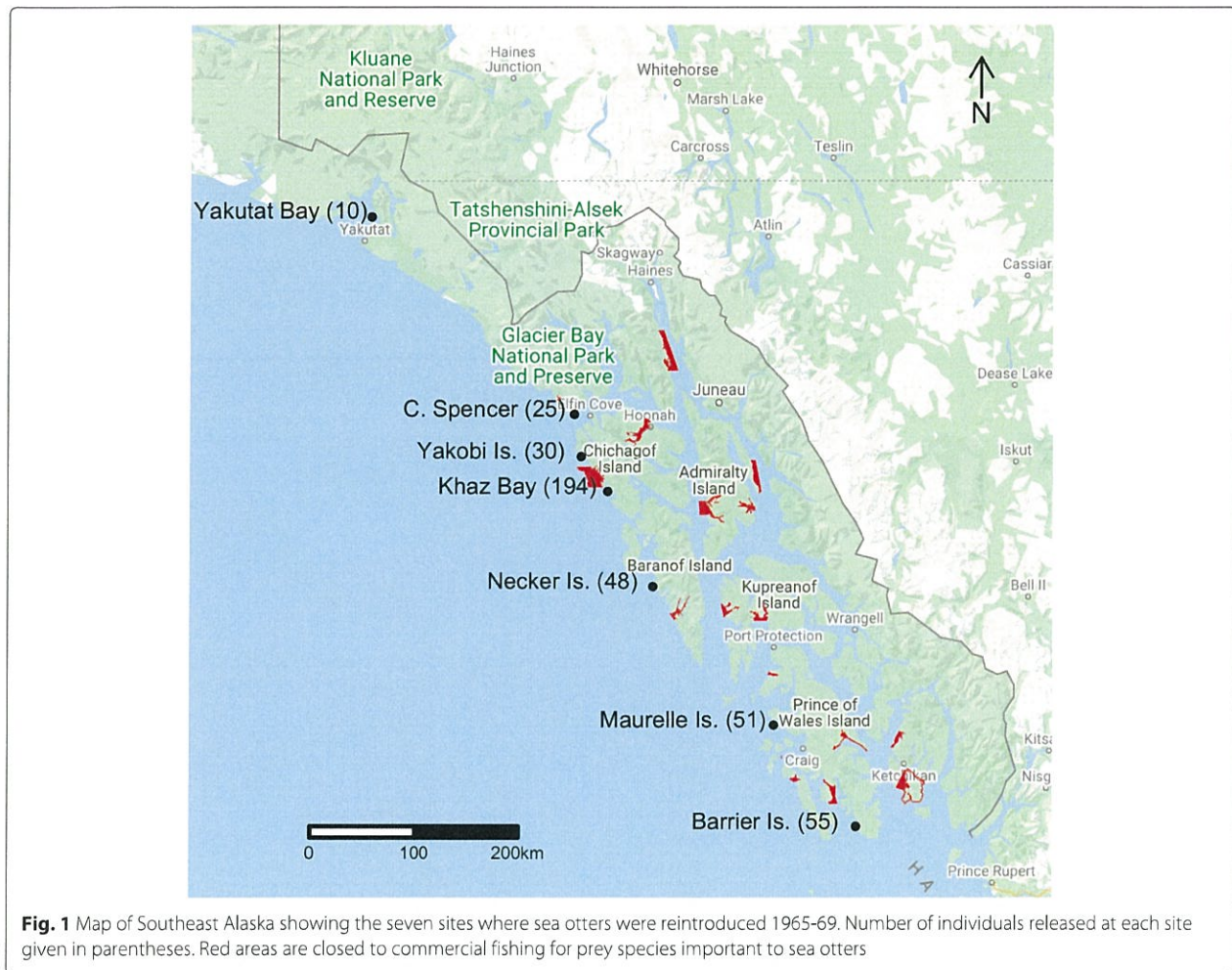
One of these areas is Southeast Alaska, where during the late 1960s, the then grazer-dominated nearshore system was perturbed by the translocation of 413 otters from stable remnant populations in Prince William Sound and around Amchitka Island, Alaska [18]. This reintroduction followed previous failed attempts and was a four-year effort that translocated sea otters to seven sites across Southeast Alaska (Fig. 1). The number of individuals released at each site ranged from 10–194 [14, 18]. These individuals seeded a population that was recently estimated to exceed 25,000 [19].

The growing and expanding population colonized previously occupied areas, as well as newly available habitat that was historically glaciated (e.g., Glacier Bay; [20]). Across Southeast Alaska, the sea otter population is likely decades from reaching carrying capacity [19, 21]; even in Glacier Bay, the most densely populated area, evidence suggests carrying capacity may not be reached for 30 years [21].

Recent studies of the sea otter population in Southeast Alaska used integrated data models to investigate regional population trends and density-dependent effects [19] and influence of subsistence harvest [22]. While the approaches applied in these studies accounted for movements between discrete sub-regions within Southeast Alaska (i.e., immigration and emigration), they assumed a known intrinsic growth rate and did not explicitly incorporate a mechanistic model of population spread that would naturally capture movements of recolonizing individuals throughout this continuous geographic area. Spatiotemporal models, including those based on ecological diffusion, allow incorporating such dynamics and can provide novel insight beyond what conventional methods yield [23]. Therefore, several questions regarding the recolonization dynamics of this and other apex predators, as well as how they drive transitions from grazer- to predator-dominated ecosystem states, remain.

For example, while wolves and their resources were protected by a national park during the early stages of their recolonization of the Greater Yellowstone Region, sea otters in Southeast Alaska faced immediate competition with commercial fishing industries for some of their primary prey (e.g., urchins *Strongylocentrotus* spp. and bivalves *Panopea* spp.) as well as mortality from subsistence harvest [24, 25]. Indeed, sea otter population growth and spread was remarkable after individuals reached Glacier Bay National Park—the only area in Southeast Alaska where subsistence harvest of sea otters is not permitted—around the mid 1980s [20], yet Southeast Alaska encompasses a diverse matrix of marine areas with various types of resource management. This recolonization event affords the opportunity to assess how natural resource management can influence predator recolonization dynamics. Further, given the multi-site nature of the reintroduction, we also have an opportunity to investigate how population growth and spread can vary among population epicenters and how multi-site reintroductions may influence the success of recolonization.

Fig. 1 Map of Southeast Alaska showing the seven sites where sea otters were reintroduced 1965-69. Number of individuals released at each site given in parentheses. Red areas are closed to commercial fishing for prey species important to sea otters

We address some of the remaining questions about predator recolonization dynamics using a mechanistic spatiotemporal model of ecological diffusion that accounts for density dependent population growth and the spread of the population from multiple reintroduction sites. In particular, we examined the growth and spread of sea otters in Southeast Alaska to (1) investigate how colonizing individuals moved throughout the area from multiple reintroduction sites and (2) determine what factors contributed to the long term persistence of sea otters in particular locations, with a focus on the influence of managed areas (e.g., where limited or no commercial fisheries exist and/or where subsistence harvest of sea otters does not occur). Our approach involved integrating the mechanistic model of population growth and spread in a Bayesian hierarchical framework to estimate process parameters and uncertainty [26]. This approach has previously been applied on much smaller spatial scales to model sea otter recolonization

and population dynamics in Glacier Bay from a single epicenter [20, 21, 27]. Here, we applied it across seven population epicenters (or reintroduction sites) to learn about changes in distribution and abundance of sea otters in a region with spatially-variable management regimes.

Methods
Data collection
Various aerial survey methods have been used to collect data on the distribution and abundance of sea otters in Southeast Alaska. These include design-based, distribution, and model-based aerial photographic surveys.

Design-based surveys Design-based aerial surveys [28, 29] were implemented in Yakutat Bay in 1995 and 2005, Glacier Bay in 1999–2004, 2006, and 2012 [30], and across the remainder of Southeast Alaska in 2002, 2003, 2010, and 2011 [31]. These surveys involved observers counting

Eisaguirre *et al. Movement Ecology*   (2021) 9:34

Page 4 of 14

sea otters along 400-m wide linear transects flown with single-engine high-winged aircraft at a speed of 104 km/hr and altitude of 91 m. Transects were stratified based on depth and distance to shore, where areas with depths ≤ 40 m and closer to shore received greater sampling effort.

These design-based surveys also incorporated intensive search units (ISUs) to use in estimating detection probability; sea otters frequently dive beneath the surface to forage, during which time that are not available for detection [27]. During the survey, approximately every 15 minutes, an ISU was initiated based on the presence of a group of 1–20 sea otters. After being counted initially, the ISUs were re-counted while the pilot flew five concentric 400-m diameter circles so that a final count of each group could be obtained. In total, greater than 20,000 km of transects were flown across Southeast Alaska, and details of this effort were outlined recently by [19].

Distribution surveys We used data from distribution surveys only when design-based data were unavailable. This included Glacier Bay in 1993, 1996–1998, 2005, 2009, and 2010. Distribution surveys were conducted by fixed-wing aircraft with one or more observers and focused on favorable marine habitats (i.e., areas where depth was < 40 m; [20]). The locations and counts of all groups of sea otters encountered were recorded by the observer(s).

Aerial photographic surveys Aerial photographic surveys [32] were conducted in Glacier Bay in 2017, 2018, and 2019 [33]. Aerial photographic surveys were conducted from a single-engine high-winged aircraft with a high-resolution DSLR camera (Nikon D810, 36.6 megapixel) with an 85 mm focal length lens (Zeiss F/1.4 ZF.2) mounted in a porthole in the belly of the aircraft. Random and optimized (see [34]) linear transects were flown at a speed of 157–166 km/hr and altitude of 213–250 m with the camera capturing overlapping images. Each image covered ~60 m ×90 m area of the water's surface. We used only non-overlapping images for analyses [21].

Hierarchical model of ecological diffusion
We modeled the growth and spread of sea otters across Southeast Alaska using an ecological diffusion model. Ecological diffusion of a population through space and time emerges from the movements of many individuals following random walks with spatially heterogeneous movement probabilities [35]. Over time, individuals congregate in favorable areas, where they exhibit longer residence time, giving rise to spatiotemporal variability in population distribution and abundance.

Model specification
We modeled sea otter abundance in Southeast Alaska at locations $i = 1, \ldots, q$, where q is the total number of 400 ×400 m grid cells in the study area, during time $t = 1970, \ldots, 2020$. Note that modeling on this 400 m spatial resolution matches the resolution of the design-based surveys. Due to the finer spatial resolution, the aerial photographic survey counts were aggregated to the 400 m scale, following [21]. Due to imperfect detection and availability of sea otters during surveys, we modeled the relationship between the latent true abundance of sea otters $N_{i,t}$ and observed relative abundance $y_{i,t}$ as

$$y_{i,t} \sim \text{Binomial}(N_{i,t}, p_t), \tag{1}$$

where p_t is the detection probability, defined here as the probability that an animal is on the surface and available to be counted. ISU data were collected during 12 years of the design-based surveys, allowing estimation of detection probability. Additionally, we used a moment-matched prior for three years for which aerial photo surveys were conducted; the moments were matched to the marginal posterior of the detection probability estimated by [34] (see Appendix 1).

We modeled true abundance with a negative binomial distribution conditioned on a dynamic mean $\lambda_{i,t}$ and dispersion parameter τ:

$$N_{i,t} \sim \text{NB}(\lambda_{i,t}, \tau). \tag{2}$$

The intensity parameter, $\lambda_{i,t}$ is the expected sea otter abundance in the ith grid cell during time t. Because diffusion is a continuous process, we obtain $\lambda_{i,t}$ by integration over a location S_i

$$\lambda_{i,t} = \int_{S_i} \lambda(\mathbf{s}, t) d\mathbf{s}, \tag{3}$$

where $\lambda(\mathbf{s}, t)$ is the population intensity at any location $\mathbf{s} \equiv (s_1, s_2)'$ in the continuous spatial domain.

We modeled the spatiotemporal dynamics to account for spread and density-dependent growth of the sea otter population with the following reaction-diffusion equation [21]:

$$\frac{\partial}{\partial t}\lambda(\mathbf{s}, t) = \left(\frac{\partial^2}{\partial s_1^2} + \frac{\partial^2}{\partial s_2^2}\right)\delta(\mathbf{s})\lambda(\mathbf{s}, t) + \gamma\lambda(\mathbf{s}, t)\left(1 - \frac{\lambda(\mathbf{s}, t)}{K(\mathbf{s})}\right). \tag{4}$$

The diffusion coefficients $\delta(\mathbf{s})$ represent motility and are inversely proportional to residence time [35, 36]. The parameter γ is the intrinsic population growth rate, and $K(\mathbf{s})$ accounts for density-dependence that may vary over

space. While $\delta(\mathbf{s})$ controls how the population spreads, $K(\mathbf{s})$ controls how many individuals areas can sustain long term. Note that $K(\mathbf{s})$ corresponds to local density dependence, and the nominal carrying capacity of the region can be obtained by $\int_{\mathcal{S}} K(\mathbf{s})d\mathbf{s}$ [21].

Equation (4) requires specifying an initial condition for $\lambda(\mathbf{s}, t_0)$. A scaled Gaussian kernel can represent a single epicenter from which a population spreads [37]. However, given that sea otters were reintroduced at seven sites throughout Southeast Alaska, we used a sum of $J = 7$ scaled Gaussian kernels, each centered on a reintroduction site (or epicenter) $\mathbf{d}_j$:

$$\lambda(\mathbf{s}, t = 1970) = \sum_{j=1}^{J} \frac{\theta_j \exp\left(\frac{-||\mathbf{s}-\mathbf{d}_j||^2}{\kappa_j^2}\right)}{\int_{\mathcal{S}} \exp\left(\frac{-||\mathbf{s}-\mathbf{d}_j||^2}{\kappa_j^2}\right) d\mathbf{s}}. \quad (5)$$

θ_j is a scale parameter controlling the initial density of individuals at $\mathbf{d}_j$, and κ_j is a dispersion parameter controlling the initial isotropic spread of those individuals around $\mathbf{d}_j$. To limit population spread based on sea otter biology, we used a reflective boundary, which does not allow population spread past the boundary, at locations adjacent to terrestrial environments as well as at locations at the offshore edge of the nearshore system, i.e., locations exposed to open ocean that are 5 km from shore or exhibit depths > 100 m, based on the distribution of survey observations.

To complete the specification of the hierarchical model, priors were specified for all model parameters. We used a combination of informative and weakly informative priors, based on previous results (e.g., from [20], [21], and [19]) as well as records of the translocations and historical observations [18]. We provide a complete list of priors in Appendix 1.

Environmental covariates
We expected that, over time, sea otters would congregate in areas with favorable habitat and resources. Thus, we modeled motility $\delta(\mathbf{s})$ as a log-linear function of covariates that have been found to be important drivers of sea otter space use and behavior [20, 21]. Based on previous studies, our covariates included depth, as a binary indicator (depth = 1 where < 40 m, and 0 otherwise), distance to shore, slope of the ocean floor, and shoreline complexity [20, 38–41]. Shoreline complexity was calculated for each location by summing the number of locations within a 1,000 m neighborhood that contained shoreline [20]. Given that subsistence harvest of sea otters [22] and human activities (e.g., disturbance from vessel traffic; [24]) influence sea otter population dynamics, we added a covariate of cumulative distance to the nearest incorporated city, town, or village. This was the sum of the shortest

swimmable paths from each city, town, or village, to any location $\mathbf{s}$.

As one of our goals was to investigate the varying levels of resource management across Southeast Alaska on the recolonization, we included Glacier Bay and fisheries closures as two indicator covariates, representing management categories. Sea otter population growth and recolonization dynamics are unique in Glacier Bay [19–21], which lies within a national park where various human activities (e.g., commercial fishing, subsistence harvest of sea otters, etc.) are limited. Some commercial fishing still occurs in Glacier Bay (i.e., for some finfish and Tanner crab *Chionoecetes bairdi*), but it is limited and being phased out. Red sea urchins (*Strongylocentrotus franciscanus*), sea cucumbers (*Parastichopus californicus*), and geoduck clams (*Panopea generosa*) are important prey for sea otters in Southeast Alaska [42–44], but they also support lucrative commercial fisheries [45]. Management of these state fisheries in Southeast Alaska involves a rotation of open and closed areas, in addition to areas that have remained closed long term due to federal jurisdiction, research, or being deemed not viable to support commercial harvest [45]; these areas closed long-term by regulation comprised what we termed 'fisheries closures' (Fig. 1). Dungeness crab (*Cancer magister*) are also important prey that are commercially harvested [46]; however, spatial data for this fishery were not available (but, we note that many of the Dungeness crab closures overlapped closures that we included). The log-linear function for motility was therefore

$$\begin{aligned}\log(\delta(\mathbf{s})) = {} & \beta_0 + \beta_1 \text{depth}(\mathbf{s}) + \beta_2 \text{dist}(\mathbf{s}) + \beta_3(\text{slope}(\mathbf{s}) \\ & \times \text{depth}(\mathbf{s})) + \beta_4 \text{shore}(\mathbf{s}) + \beta_5 \text{town}(\mathbf{s}) \\ & + \beta_6 \text{glba}(\mathbf{s}) + \beta_7 \text{fish}(\mathbf{s}).\end{aligned}$$
$$(6)$$

While modeling $\delta(\mathbf{s})$ as a function of covariates allows for investigating how the population spreads to reach certain areas, modeling local density dependence $K(\mathbf{s})$ allows us to see if certain areas may influence long term population dynamics and densities. So, to further allow the process model to have sufficient flexibility to capture the unique colonization dynamics of Glacier Bay and to investigate the effects of resource management, including fisheries closures, on sea otter population dynamics within the ecological diffusion framework, we allowed density dependence to vary over space as a function of covariates. This took the form:

$$\log(K(\mathbf{s})) = \alpha_0 + \alpha_1 \text{glba}(\mathbf{s}) + \alpha_2 \text{fish}(\mathbf{s}). \quad (7)$$

While this formulation implies local density dependence (or local nominal carrying capacity) varies over the region

only according to these two indicator covariates, realized carrying capacity depends on motility and thus the covariates driving it as well [21].

All covariates, except for the binary indicators, were centered and scaled to mean zero and unit variance for estimation.

Estimation, derived parameters, and model validation

We sampled from the posterior distribution of the hierarchical model with Markov chain Monte Carlo (MCMC), implemented in R and C++ [47]. Ecological diffusion (Eq. 4) is continuous in space and time, so we used finite differencing for estimation over the discretized spatial and temporal domains [21, 27, 36]. Due to the resolution of the data, we set the spatial discretization to 400 m ×400 m and the temporal discretization to $\Delta t = 1$ d. Additionally, we used homogenization for computational feasibility [21, 27, 36, 48], which was described in detail by [21] for the logistic ecological diffusion model. We followed [27] and [21] and chose $\epsilon = 1/10$, which corresponds to a homogenized scale of 4 km ×4 km. Much of the computational demand of this and similar spatiotemporal models results from the high dimensional matrix operations required by the finite differencing procedure [27]. In contrast to previous work, we handled those as sparse matrix operations, which reduced the computational burden markedly.

To help understand how the colonization front of otters moved through space and time, we estimated the asymptotic spatially explicit spread (or colonization) rates. The asymptotic spread rate for the Malthusian (or exponential growth) model and the minimum spread rate for the logistic model is given by $2\sqrt{\bar{\delta}\gamma}$, where $\bar{\delta}$ is the homogenized diffusion coefficient [20, 49]. Asymptotic spread rates greater than the minimum are allowed in nonlinear (e.g., logistic) cases, and computing them requires knowing the shape of the wave front. From Eq. (5), the steepness of the front at $t = 1970$ is $1/\kappa_j^2$, and from theory of propagating waves, we know that the shape of the wave front is conserved [50]. Finally, if the front is steep, i.e., $1/\kappa_j^2 > \sqrt{\gamma/\bar{\delta}}$, then the spread rate converges to $2\sqrt{\bar{\delta}\gamma}$, whereas if the front is flat, i.e., $1/\kappa_j^2 < \sqrt{\gamma/\bar{\delta}}$, asymptotic spread rate can be computed as $\frac{\bar{\delta}}{\kappa_j^2} + \gamma\kappa_j^2$ for any time $t > 1970$ [50, 51].

We estimated total abundance $N(t) = \int_S N(\mathbf{s}, t)d\mathbf{s}$ by

$$N^{(k)}(t) = \sum_{i=1}^{n_{0,t}} N_{i,t} + \sum_{m=1}^{n_t - n_{0,t}} \hat{N}_{m,t}^{(k)} + \sum_{l=1}^{q - n_t} \tilde{N}_{l,t}^{(k)} \qquad (8)$$

for the kth MCMC iteration. The term $N_{i,t}$ is an observation of true abundance, $\hat{N}_{m,t}^{(k)}$ is posterior draw of true abundance where relative abundance was observed,

$\tilde{N}_{l,t}^{(k)} \sim \text{NB}(\lambda_{l,t}^{(k)}, \tau^{(k)})$ where no data were collected, n_t is the number of locations where relative abundance or true abundance was observed, and $n_{0,t}$ is the number of locations where only true abundance was observed [21].

We used the posterior predictive distribution to assess model fit. A posterior predictive draw for an observation $y_{i,t}$ is given by $\tilde{y}_{i,t}^{(k)} \sim \text{Binomial}(\tilde{N}_{i,t}^{(k)}, p_t^{(k)})$. We compared these samples to the data point-wise by comparing the observed counts to the 95% credible intervals of the posterior predictive counts [52]. We assessed convergence to the posterior by visual inspection of the MCMC chains with traceplots. We summarized our parameter estimates using posterior means and 90% credible intervals [53, 54].

Results

It required approximately seven days using 15 independent chains run in parallel to obtain an MCMC sample of 15,000 iterations from the posterior. Only 23 of 42,553 observed counts fell outside of the 95% posterior predictive intervals, suggesting no lack of fit over the area that was surveyed.

We estimated an intrinsic growth rate of about 0.29 (0.28, 0.31; Table 1). Our estimates of total abundance (Fig. 2) were similar to other recent estimates [19] and those obtained with the design-based estimator [55]. Although not definitive, it appears the consistently high annual growth rate of the sea otter population across Southeast Alaska may have begun to slow in the last few years (Fig. 2).

We also found evidence that all covariates included in the model had an effect on the spatiotemporal process, both in terms of motility and density dependence (Table 1). Generally, sea otters across Southeast Alaska seemed to prefer areas with shallow depth (i.e., < 40 m), close to shore, steeper slopes (in areas with shallow depth), and straighter shorelines (Table 1). Additionally, sea otters tended to concentrate in Glacier Bay, areas with fisheries closures, and areas close to human communities, although the effect size was relatively large for areas with fisheries closures compared to Glacier Bay and human communities (Table 1). Further, population densities that begin to regulate growth were likely highest in Glacier Bay, followed by areas with fisheries closures, and lowest elsewhere in the region, although there was overlap in credible intervals between the effects of the protected status of Glacier Bay and areas with fisheries closures (Table 1).

The initial dispersal conditions suggested a steep wave front (i.e., satisfied $1/\kappa_j^2 > \sqrt{\gamma/\bar{\delta}}$), so we estimated asymptotic spread rates with $2\sqrt{\bar{\delta}\gamma}$ across all epicenters. Rates varied primarily from about 1–8 km/yr, with a median of 3.0 km/yr, but areas further from shore commonly exhibited more rapid spread rates (Fig. 3).

Eisaguirre *et al. Movement Ecology*   (2021) 9:34

Page 7 of 14

Table 1 Posterior means and 90% credible intervals for the parameters of the ecological diffusion model with logistic growth estimated for the sea otter population in Southeast Alaska 1970 to 2020. The subscripts on θ and κ are abbreviations of the translocation sites shown in Fig. 1. Estimates of detection probabilities are provided in Appendix 2: Table 2

Parameter	Lower bound	Mean	Upper bound
β_0 (intercept)	16.25	16.36	16.48
β_1 (depth)	-1.89	-1.77	-1.66
β_2 (distance to shore)	0.21	0.29	0.35
β_3 (slope × depth)	0.14	0.22	0.29
β_4 (shoreline complexity)	0.14	0.17	0.21
β_5 (distance to towns)	0.37	0.45	0.55
β_6 (Glacier Bay)	-0.37	-0.24	-0.10
β_7 (fisheries closures)	-1.48	-1.34	-1.16
α_0 (intercept)	-1.77	-1.66	-1.55
α_1 (Glacier Bay)	2.78	3.16	3.58
α_2 (fisheries closures)	0.12	1.87	6.91
γ (intrinsic growth)	0.28	0.29	0.31
τ (overdispersion)	0.03	0.03	0.03
θ_{MI} (initial density)	119.65	147.53	175.46
θ_{BI}	8.06	9.75	11.40
θ_{NI}	8.33	9.96	11.63
θ_{KB}	65.41	98.90	132.59
θ_{YB}	8.36	10.01	11.69
θ_{YI}	63.74	96.18	128.84
θ_{CS}	68.19	98.82	130.55
κ_{MI} (initial dispersal)	25.41	28.78	32.20
κ_{BI}	1.37	2.54	3.80
κ_{NI}	4.42	9.11	13.90
κ_{KB}	0.51	0.63	0.78
κ_{YB}	0.80	2.23	3.79
κ_{YI}	4.17	8.49	12.40
κ_{CS}	4.59	9.23	13.91

Additionally, areas with fisheries closures generally exhibited slower spread rates (Fig. 3).

Discussion

To improve our understanding of the reintroduction biology of apex predators [13], we modeled the ongoing recolonization of Southeast Alaska by sea otters as a spatiotemporal process based on ecological diffusion, accounting for multiple population epicenters (i.e., reintroduction sites), preferential dispersal, and spatially-variable density dependence (Fig. 4). In addition to the novelty of spatially-varying density dependence, to our knowledge, this is the largest spatial extent and finest spatial reso-
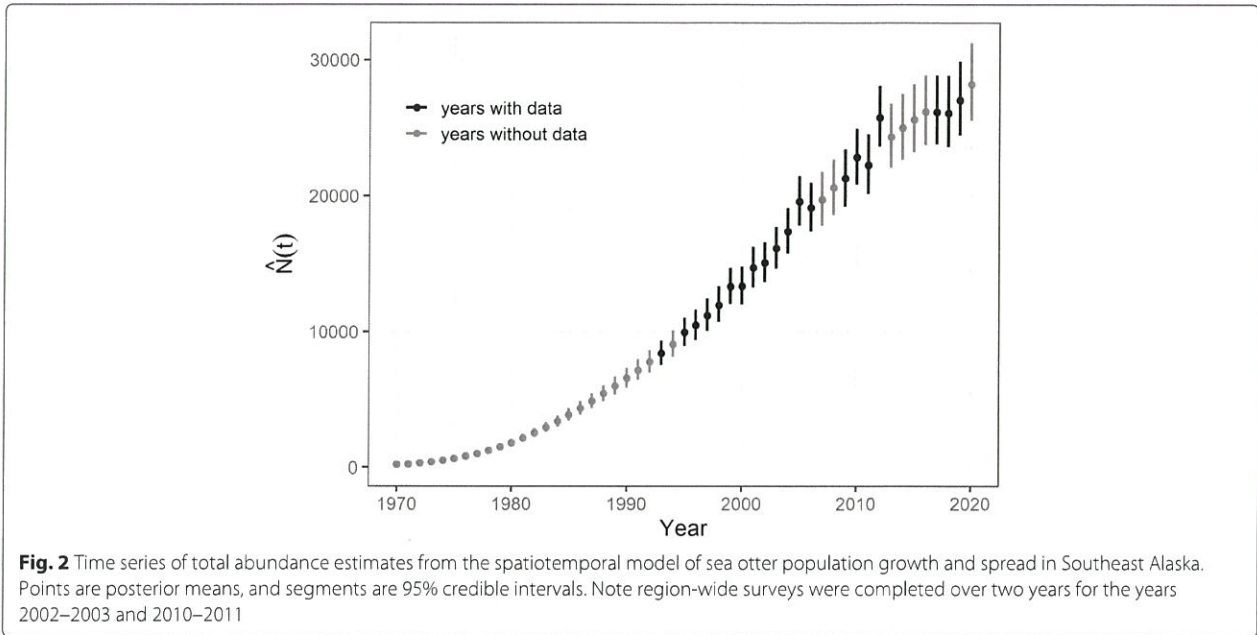
lution over which such a model has been implemented. Homogenization offers substantial computational gains [36, 48], but we also used sparse matrix operations, which made implementing the model on the scale of Southeast Alaska much more computationally tractable.

Ecological diffusion is well established in mathematical and ecological theory pertaining to the spread of organisms [35]; however, other process models could certainly be used to model recolonizing populations. For example, [56] implemented a dynamic occupancy model where colonization proceeds following gradients of favorable habitat. While an extension to modeling abundance in their framework is certainly possible, ecological diffusion naturally models abundance as well as movement toward and concentration in favorable habitat. [19] and [38] modeled sea otter recolonization (of Southeast Alaska and the central coast of California, respectively) by parsing the study areas into distinct units and specifying immigration and emigration among them. While doing so offers computational advantages, inferences are restricted to those defined units. In contrast, with a continuous spatiotemporal model, such as ecological diffusion, inferences can be made about any areas of interest within the modeled domain—defined a priori or *a posteriori*—based on straightforward *post hoc* calculations (e.g., time series of abundance within different areas).

Our results from applying the ecological diffusion model to Southeast Alaska indicate that sea otters generally concentrate in areas presumed to be favorable for foraging as well as areas closer to human communities, but sea otter densities that begin to regulate population growth are higher in areas with limited or no commercial fishing and other human activities. We were also able to obtain greater precision in our estimates of total abundance than design-based estimators and recent modeling efforts (Fig. 2; [19]). Furthermore, we found that the rates of colonization averaged about 3 km/yr throughout the region, with higher rates being in areas with higher motility. These factors all contributed to the ongoing success of the recolonization that continues to drive ecosystem change in the region [15, 42].

Spatial variability in abundance

Another effort to model the growth and expansion of the sea otter population in Southeast Alaska found that abundance and carrying capacity varied between large, discrete sub-regions [19]. However, we also accounted for how spatial covariates drive variation in abundance and movement of sea otters throughout the region (Figs. 3 & 4). We found that shallow depth, which defines foraging habitat [39, 40], was positively correlated with sea otter residence time. We also found that sea otters additionally concentrate in areas where commercial fisheries are closed, as well as in protected areas, where subsistence harvest of

Fig. 2 Time series of total abundance estimates from the spatiotemporal model of sea otter population growth and spread in Southeast Alaska. Points are posterior means, and segments are 95% credible intervals. Note region-wide surveys were completed over two years for the years 2002–2003 and 2010–2011
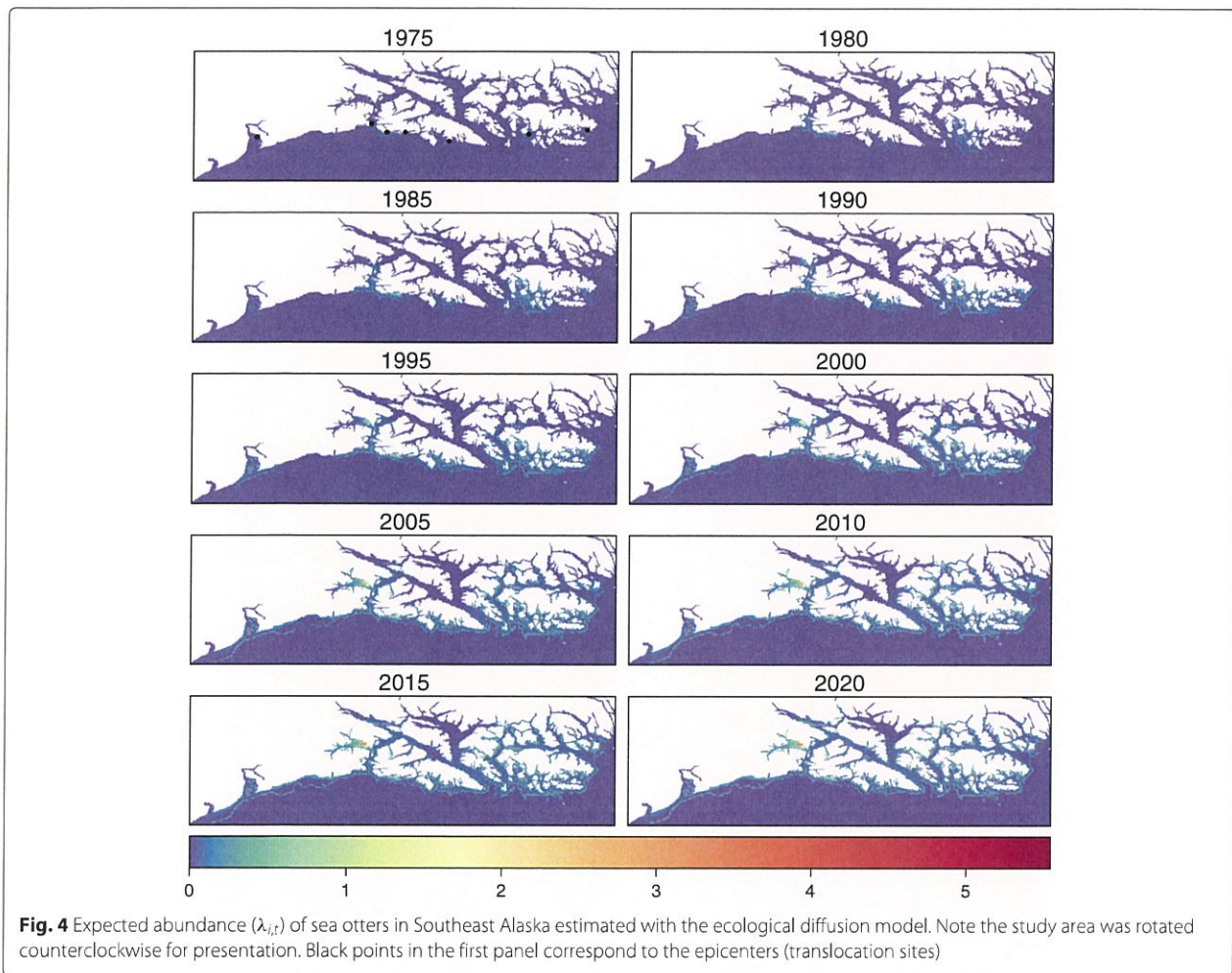
sea otters is not permitted (i.e., Glacier Bay; Table 1), which suggests greater prey availability, foraging habitat, and mortality risk are strong drivers of sea otter distribution and abundance. Our finding that sea otters exhibit higher residence time closer to human communities is seemingly inconsistent with previous findings of exposure to subsistence hunting influencing sea otter movement [44] and population growth [22]. However, the diffusion model is likely capturing what happens during the initial

colonization of areas closer to communities, and, in the longer-term, areas closer to communities where harvest is common may act as population sinks [22].

Sea otter colonization and foraging habits have marked effects on assemblages of benthic invertebrates, including many commercially-harvested shellfish [42, 44, 57]. While some areas are closed to commercial fishing in Southeast Alaska due to seemingly unsupportable abundances of harvested species (for commercial purposes), sea otters

Fig. 3 Asymptotic spread rates of the sea otter population in Southeast Alaska based on parameters estimated in the ecological diffusion model. Note that the map is presented on the homogenized (4 km) resolution, and the red points represent the epicenters (translocation sites). On the left is a histogram showing the values presented in the map on the right. Note the *x*-axis is truncated for presentation. Red vertical lines represent the spread rates in areas closed to commercial fishing for prey species important to sea otters

Eisaguirre *et al. Movement Ecology*   (2021) 9:34

Page 9 of 14

Fig. 4 Expected abundance ($\lambda_{i,t}$) of sea otters in Southeast Alaska estimated with the ecological diffusion model. Note the study area was rotated counterclockwise for presentation. Black points in the first panel correspond to the epicenters (translocation sites)

are adept at capturing these species even in closed areas. [42] found that sea cucumber abundance negatively correlates with sea otter occupancy but also observed sea cucumbers in sea otter diets in areas where surveys suggested a 100% decline in sea cucumbers. This finding suggests that sea otters can find prey even when it is undetected by targeted surveys. So, even in areas that may not be able to support commercial harvest by humans, an abundance of prey may be available to sea otters, including sea cucumbers but likely other species as well that may have become abundant as the ecosystem transitioned to the predator-dominated state [58].

In addition to influencing residence time of sea otters, these areas with reduced commercial activity may offer sea otters some relief from competition for food resources, thereby supporting the higher nominal carrying capacities suggested by our results (Table 1). Furthermore, extensive glacial retreat over the last 350 years and subsequent ecological succession in the marine

environment has led to a highly diverse and abundant benthic prey community in Glacier Bay since sea otters previously inhabited the region [20, 57]. In addition to the reduced human activity in the protected area of Glacier Bay, the new habitat likely further contributed to the higher nominal carrying capacity there (Table 1; [19, 21]). As the population expands into other previously-glaciated fjords with shallow habitat, we might expect such areas to similarly support higher carrying capacities, and we may be presented with an opportunity to investigate how novel niche space might interact with management strategy to drive spatially-variable carrying capacities.

In contrast to the relatively rapid recolonization of Southeast Alaska, sea otter populations have been slower to recover in the southern parts of their range, such as the coastal habitat of California. Parts of Southeast Alaska, such as the outer coast, are dominated by rocky benthos that can support healthy kelp forests. So, the top-down

effects on grazers by sea otters would quickly release kelp from control [16], in turn providing otters with protective habitat. The California coast, on the other hand, is a matrix of disjunct rocky benthos and stretches of softer substrate—poor for persistent kelp forest establishment—that may limit the recovery of sea otter populations via limiting female dispersal and survival [59, 60]. Further, much more of the nearshore marine environment in California is exposed to open ocean compared to the more sheltered bays and passages of Southeast Alaska. Particularly exposed areas of the California coast (e.g., Point Conception) are thought to be barriers to sea otter population spread [60], and new evidence suggests sea otters may have utilized protected estuaries historically [61]. Predation by white sharks (*Carcharodon carcharias*) may also limit sea otter range expansion along the California coast [62]. These regional differences in recolonization dynamics highlight the need to carefully consider strategies to improve the likelihood of long-term success of predator reintroduction efforts.

Other studies have included multiple fine scale habitat covariates in population models to explain carrying capacity of sea otters [38]. As more spatial data become available for Southeast Alaska, similar covariates could be included in the diffusion model. However, homogenization of the logistic diffusion model implies that realized carrying capacity is, in part, a function of motility [21]. We included two indicator covariates in our formulation of $K(\mathbf{s})$, representing areas with different management regimes, but variation in motility over the region also explains spatial variation in carrying capacity in the model. Other covariates, such as kelp canopy cover and benthic substrate composition, which have been shown to be important drivers of sea otter carrying capacity elsewhere [38], could be included in future models (i.e., as covariates affecting density dependence and/or motility).

Colonization rates and multi-site reintroductions

While we estimated a median spread rate of 3.0 km/yr in Southeast Alaska, we also found that asymptotic spread rates of sea otters can vary greatly over such a vast region (Fig. 3). Asymptotic spread rates of recolonizing sea otters in California were first estimated to range from about 1.7 to 3.5 km/yr [63], and [60] estimated about 4.7 km/yr for the southern edge of the California range and about 2 km/yr for the northern edge. Similarly, [20] estimated rates of 1.5 to 4.5 km/yr in Glacier Bay. Recalling that these spread rates are estimated as $2\sqrt{\bar{\delta}\gamma}$ [20, 49, 63], the greater range that we estimated is due to (1) a higher intrinsic growth rate (discussed below; Table 1), as well as (2) the extensive spatial variability in motility harbored by a region of such size.

While we did not find evidence that any of the initial dispersal conditions (i.e., κ_j) for sea otters in Southeast Alaska affected the theoretical asymptotic spread rates (Table 1), and thus the spatial variation of those rates did not vary among epicenters (Fig. 3), specific translocation strategies could improve colonization rates. For example, if individuals were released at a site such that they were spread out sufficiently to create a flat propagating front (i.e., satisfying the condition $1/\kappa_j^2 < \sqrt{\gamma/\bar{\delta}}$), theory suggests the population could spread at rates greater than the minimum spread rate (i.e., $\frac{\bar{\delta}}{\kappa_j^2} + \gamma\kappa_j^2$; [50, 51]). Somewhat counter-intuitively, this suggests that higher colonization rates could be achieved by reintroducing individuals over wide areas where the species is expected to have higher motility and thus lower residence time (i.e., less favorable habitat). While it is important to note that failed reintroductions are commonly attributed to translocations of low initial densities (resulting in elevated effects of demographic stochasticity and/or Allee effects) and to unsuitable habitat (causing high mortality; [13]), individuals released in areas correlating with low residence time should spread rapidly to several locations with more favorable habitat and begin to concentrate in those areas. In fact, our results provided evidence of this: The sea otter population spread quickly over areas with high motility, then settled at high abundance in areas with low motility, which included areas with limited or no commercial fishing (Figs. 3 & 4). Given the relationship between motility in the ecological diffusion model, population spread rates, and specific forms of resource selection functions [64], it is possible that preliminary investigations of individual animal movement—either in the reintroduction area or a similar area—could be used to optimize a reintroduction strategy in terms of the initial locations and densities of released individuals. Nonetheless, these inferences regarding improved translocation strategies are largely based on mathematical theory underlying diffusion models, so further study is needed to determine how they may apply to translocation and reintroduction efforts in practice.

While sea otter reintroductions along the North American coast were an early example of a multi-site effort [18], there is a recent and ongoing multi-site reintroduction of a terrestrial predator, fisher (*Pekania pennanti*), in the northwestern U.S. [65]. Similar to sea otters, fishers declined due to over-harvest and lack of management, yet reintroduction attempts have been showing promise in restoring this predator across its historical range [10]. The simulation modeling by [10] suggested that multiple reintroduction sites can improve the success of predator recolonization. Our work adds to this body of knowledge by documenting, with a mechanistic model fit to data, how

such a process occurs over a region where colonizing individuals face variability in motility and density dependence. Indeed, our application was to a marine system, although a parallel application to the expanding fisher populations or similar terrestrial predator could reveal how such a process might vary between marine and terrestrial systems, over which animals have inherent differences in motility. Nonetheless, we found the spread rates of sea otters in Southeast Alaska were generally less than the 9.78 km/yr documented for wolves—highly mobile terrestrial predators [8]. Although, in certain areas, sea otter populations may be able to exceed that rate (Fig. 3).

Intrinsic growth

A maximum growth rate of about 20–25% has been generally accepted for sea otter populations for some time [19, 66]. However, modeling the growth and spread of sea otters across the entire region of Southeast Alaska as a continuous spatiotemporal process suggested intrinsic growth for at least this population is higher (Table 1). The evidence was quite strong: We used an informative prior for γ centered on 0.25, based on previous studies, yet the data easily pulled the marginal posterior upward (Table 1; Appendix 1).

While the previous estimates were generally accepted, it had been suggested they were likely biased low due to underestimated natality [67]. Assuming female sea otters in the area have the ability to average about one female pup every other year, our estimated intrinsic growth of about 0.29 is reasonable and aligns with the requisite theoretical maximum population growth rate [66, 68]. It is therefore possible that sea otter populations have the potential to grow more rapidly when unhindered by density-dependent factors than previous evidence suggested. Indeed, our estimate of intrinsic growth is high among marine mammals [66, 69, 70] but is reasonable, especially because the relatively mild winter conditions and productivity of Southeast Alaska are likely conducive to sea otters averaging one pup per year.

Application of a diffusion model similar to the one we implemented revealed the intrinsic growth rate of wolves colonizing parts of France varied between about 0.3 and 0.7, depending on the amount of forest cover [71]. However, modeling intrinsic growth—the theoretical maximum rate of increase of the population—as a function of covariates, as [71] did, implicitly assumes that those covariates have a density-independent effect on population growth. In contrast, we chose to model the density dependence parameter $K(\mathbf{s})$ as a function of spatial covariates because we hypothesized those covariates would affect how density moderates population growth (e.g., through reduced prey availability at higher population densities), rather than be density-independent.

Continued population growth and spread

While it appears the annual rate of increase of the sea otter population in Southeast Alaska may be slowing (Fig. 2), it is likely still decades from reaching total carrying capacity [19, 21]. As the recolonization process continues, the population will reach new habitat, in addition to Glacier Bay, that will similarly afford greater local equilibrium abundances. Sea otters in the region also face growing conflicts with human interests and activities due to their effects on commercially-valuable and subsistence species [25]. However, the return of the historical state of the nearshore marine ecosystem is gaining support among many stakeholders because there is great value in the ecosystem services that the predator-dominated system can render, such as improved carbon sequestration, nursery habitat for fish, and greater fish biomass [6, 72].

As we continue to monitor this growing and expanding population, as well as the requisite ecosystem change, we can adapt our modeling approach to gain additional insight into total equilibrium abundance, the spatial variability of equilibrium abundance, the effects of subsistence harvest of sea otters and commercial fisheries, and how climate change may continue to influence the process. Key to this ongoing effort will be using the mechanistic diffusion model to forecast population growth and spread to dynamically optimize the monitoring framework (*sensu* [34]).

Conclusions

As predator reintroductions continue to be proposed (e.g., 2020 Colorado Proposition 114), there is an increasing need to understand recolonization processes across modern land- and seascapes with varying levels of management and human activity. Fundamental to our understanding of how keystone predator reintroductions can drive ecosystem change is understanding how a predator population grows and expands its range. We provide new insight into how colonization and growth can occur from multiple reintroduction sites and with spatial heterogeneity in both the physical environment as well as human activity and management.

Appendix 1: Priors

$\gamma \sim \text{Normal}(0.25, 0.01^2)$
$\boldsymbol{\beta} \sim \text{Normal}(\mathbf{0}, 10^2\mathbf{I})$
$\theta_j \sim \text{Normal}^+\left(\mu_{\theta,j}, \sigma^2_{\theta,j}\right)$, where $\boldsymbol{\mu}_\theta = (100, 10, 10, 100,$ $10, 100, 100)'$ and $\boldsymbol{\sigma}^2_\theta = (20^2, 1^2, 1^2, 20^2, 1^2, 20^2, 20^2)'$
$\kappa_j \sim \text{Normal}^+(\mu_{\kappa,j}, \sigma^2_{\kappa,j})$, where $\boldsymbol{\mu}_\kappa = (10, 2, 10, 10, 2,$ $10, 10)'$ and $\boldsymbol{\sigma}^2_\kappa = (3^2, 1^2, 3^2, 3^2, 1^2, 3^2, 3^2)'$
$\tau \sim \text{Uniform}(0, 1)$
$\boldsymbol{\alpha} \sim \text{Normal}(\mathbf{0}, 10^2\mathbf{I})$
$p_t \sim \text{Beta}(1, 1)$ for $t \neq 2017, 2018, 2019$
$p_t \sim \text{Beta}(44.04937, 13.40566)$ for $t = 2017, 2018, 2019$

Eisaguirre *et al. Movement Ecology*   (2021) 9:34

Page 12 of 14

Appendix 2

Table 2 Full version of table 1 from the main text that includes detection probabilities

Parameter	Lower bound	Mean	Upper bound
β_0	16.25	16.36	16.48
β_1	-1.89	-1.77	-1.66
β_2	0.21	0.29	0.35
β_3	0.14	0.22	0.29
β_4	0.14	0.17	0.21
β_5	0.37	0.45	0.55
β_6	-0.37	-0.24	-0.10
β_7	-1.48	-1.34	-1.16
α_0	-1.77	-1.66	-1.55
α_1	2.78	3.16	3.58
α_2	0.12	1.87	6.91
γ	0.28	0.29	0.31
τ	0.03	0.03	0.03
θ_{MI}	119.65	147.53	175.46
θ_{BI}	8.06	9.75	11.40
θ_{NI}	8.33	9.96	11.63
θ_{KB}	65.41	98.90	132.59
θ_{YB}	8.36	10.01	11.69
θ_{YI}	63.74	96.18	128.84
θ_{CS}	68.19	98.82	130.55
κ_{MI}	25.41	28.78	32.20
κ_{BI}	1.37	2.54	3.80
κ_{NI}	4.42	9.11	13.90
κ_{KB}	0.51	0.63	0.78
κ_{YB}	0.80	2.23	3.79
κ_{YI}	4.17	8.49	12.40
κ_{CS}	4.59	9.23	13.91
p_{1999}	0.74	0.80	0.85
p_{2000}	0.70	0.75	0.80
p_{2001}	0.82	0.86	0.89
p_{2002}	0.86	0.89	0.91
p_{2003}	0.77	0.79	0.82
p_{2004}	0.73	0.77	0.81
p_{2005}	0.53	0.58	0.63
p_{2006}	0.71	0.75	0.78
p_{2010}	0.87	0.90	0.92
p_{2012}	0.54	0.58	0.63
p_{2017}	0.67	0.77	0.85
p_{2018}	0.67	0.77	0.85
p_{2019}	0.67	0.77	0.85

Declarations

Ethics approval and Consent to participate
Aerial surveys were conducted under U.S. Fish and Wildlife Service Scientific Research Permit #MA14762C-0 and National Park Service Scientific Research Permit GLBA-2016-SCI-022.

Consent for publication
All authors consent to publication. Any use of trade, firm, or product names is for descriptive purposes only and does not imply endorsement by the U.S. Government. The findings and conclusions of the U.S. Fish and Wildlife Service authors are their own and do not necessarily represent the views of the U.S. Fish and Wildlife Service.

Competing interests
The authors declare that they have no competing interests.

Author details
[1]Department of Natural Resources and Environmental Science, University of Nevada Reno, Reno, NV, USA. [2]United States Fish & Wildlife Service, Marine Mammals Management, Anchorage, AK, USA. [3]Department of Statistics, Colorado State University, Fort Collins, CO, USA. [4]U.S. Geological Survey, Alaska Science Center, Anchorage, AK, USA. [5]Southeast Alaska Inventory and Monitoring Network, National Park Service, Juneau, AK, USA. [6]Glacier Bay Field Station, National Park Service, Juneau, AK, USA. [7]Colorado Cooperative Fish and Wildlife Research Unit, U.S. Geological Survey, Department of Fish, Wildlife, and Conservation Biology, Colorado State University, Fort Collins, CO, USA. [8]Present address: Wildlife Biology Program, Department of Ecosystem and Conservation Sciences, W.A. Franke College of Forestry and Conservation, University of Montana, Missoula, MT, USA. [9]Present address: U.S. Geological Survey, Upper Midwest Environmental Sciences Center, La Crosse, WI, USA.

References
1. Ripple WJ, Estes JA, Beschta RL, Wilmers CC, Ritchie EG, Hebblewhite M, Berger J, Elmhagen B, Letnic M, Nelson MP, Schmitz OJ, Smith DW, Wallach AD, Wirsing AJ. Status and ecological effects of the world's largest carnivores. Science. 2014;343(6167). https://doi.org/10.1126/science.1241484.

Eisaguirre *et al. Movement Ecology*   (2021) 9:34

Page 13 of 14

2. Estes JA, Terborgh J, Brashares JS, Power ME, Berger J, Bond WJ, Carpenter SR, Essington TE, Holt RD, Jackson JBC, Marquis RJ, Oksanen L, Oksanen T, Paine RT, Pikitch EK, Ripple WJ, Sandin SA, Scheffer M, Schoener TW, Shurin JB, Sinclair ARE, Soulé ME, Virtanen R, Wardle DA. Trophic downgrading of planet Earth. Science. 2011;333(6040):301–6. https://doi.org/10.1126/science.1205106.

3. Prugh LR, Stoner CJ, Epps CW, Bean WT, Ripple WJ, Laliberte AS, Brashares JS. The rise of the mesopredator. BioScience. 2009;59(9):779–91. https://doi.org/10.1525/bio.2009.59.9.9.

4. Wallach AD, Johnson CN, Ritchie EG, O'Neill AJ. Predator control promotes invasive dominated ecological states. Ecol Lett. 2010;13(8): 1008–18. https://doi.org/10.1111/j.1461-0248.2010.01492.x.

5. Ripple WJ, Beschta RL. Trophic cascades in Yellowstone: The first 15 years after wolf reintroduction. Biol Conserv. 2012;145(1):205–13. https://doi.org/10.1016/j.biocon.2011.11.005.

6. Gregr EJ, Christensen V, Nichol L, Martone RG, Markel RW, Watson JC, Harley CDG, Pakhomov EA, Shurin JB, Chan KMA. Cascading social-ecological costs and benefits triggered by a recovering keystone predator. Science. 2020;368(6496):1243–7. https://doi.org/10.1126/science.aay5342.

7. Ritchie EG, Elmhagen B, Glen AS, Letnic M, Ludwig G, McDonald RA. Ecosystem restoration with teeth: What role for predators? Trends Ecol Evol. 2012;27(5):265–71. https://doi.org/10.1016/j.tree.2012.01.001.

8. Hurford A, Hebblewhite M, Lewis MA. A spatially explicit model for an Allee effect: Why wolves recolonize so slowly in Greater Yellowstone. Theor Popul Biol. 2006;70(3):244–54. https://doi.org/10.1016/j.tpb.2006.06.009.

9. Fischer J, Lindenmayer DB. An assessment of the published results of animal relocations. Biol Conserv. 2000;96(1):1–11. https://doi.org/10.1016/S0006-3207(00)00048-3.

10. Lewis JC, Powell RA, Zielinski WJ. Carnivore translocations and conservation: Insights from population models and field data for fishers (*Martes pennanti*). PLoS ONE. 2012;7(3):32726. https://doi.org/10.1371/journal.pone.0032726.

11. Ovenden TS, Palmer SCF, Travis JMJ, Healey JR. Improving reintroduction success in large carnivores through individual-based modelling: How to reintroduce Eurasian lynx (*Lynx lynx*) to Scotland. Biol Conserv. 2019;234(March):140–53. https://doi.org/10.1016/j.biocon.2019.03.035.

12. Seddon PJ, Griffiths CJ, Soorae PS, Armstrong DP. Reversing defaunation: Restoring species in a changing world. Science. 2014;345(6195):406–12.

13. Armstrong DP, Seddon PJ. Directions in reintroduction biology. Trends Ecol Evol. 2008;23(1):20–5. https://doi.org/10.1016/j.tree.2007.10.003.

14. Bodkin JL. Historic and Contemporary Status of Sea Otters in the North Pacific. In: Larson SE, Bodkin JL, VanBlaricom GR, editors. Sea Otter Conservation. Cambridge: Academic Press; 2015. p. 43–61. https://doi.org/10.1016/B978-0-12-801402-8.00003-2.

15. Estes JA, Duggins DO. Sea otters and kelp forests in Alaska: generality and variation in a community ecological paradigm. Ecol Monogr. 1995;65(1): 75–100. https://doi.org/10.2307/2937159.

16. Estes JA, Palmisano JF. Sea Otters: Their role in structuring nearshore communities. Science. 1974;185(4156):1058–60.

17. Estes JA, Tinker MT, Bodkin JL. Using ecological function to develop recovery criteria for depleted species: sea otters and kelp forests in the Aleutian Archipelago. Conserv Biol. 2010;24(3):852–60. https://doi.org/10.1111/j.1523-1739.2009.01428.x.

18. Jameson RJ, Kenyon KW, Johnson AM, Wight HM. History and status of translocated sea otter populations in North America. Wildl Soc Bull. 1982;10(2):100–7.

19. Tinker MT, Gill VA, Esslinger GG, Bodkin J, Monk M, Mangel M, Monson DH, Raymond WW, Kissling ML. Trends and carrying capacity of sea otters in southeast Alaska. J Wildl Manag. 2019;83(5):1073–89. https://doi.org/10.1002/jwmg.21685.

20. Williams PJ, Hooten MB, Esslinger GG, Womble JN, Bodkin JL, Bower MR. The rise of an apex predator following deglaciation. Divers Distrib. 2019;25(6):895–908. https://doi.org/10.1111/ddi.12908.

21. Lu X, Williams PJ, Hooten MB, Powell JA, Womble JN, Bower MR. Nonlinear reaction–diffusion process models improve inference for population dynamics. Environmetrics. 2020;31(3):2604. https://doi.org/10.1002/env.2604.

22. Raymond WW, Tinker MT, Benter B, Kissling M, Gill VA, Eckert GL. Location-specific factors influence patterns and effects of subsistence sea otter harvest in Southeast Alaska. Ecosphere. 2019;10(September):e02874.

23. Hefley TJ, Hooten MB, Russell RE, Walsh DP, Powell JA. When mechanism matters: Bayesian forecasting using models of ecological diffusion. Ecol Lett. 2017;20(5):640–50. https://doi.org/10.1111/ele.12763.

24. Ballachey BE, Bodkin JL. Challenges to Sea Otter Recovery and Conservation. In: Larson SE, Bodkin JL, VanBlaricom GR, editors. Sea Otter Conservation. Cambridge: Academic Press; 2015. p. 63–96. https://doi.org/10.1016/B978-0-12-801402-8.00004-4.

25. Carswell LP, Speckman SG, Gill VA. Shellfish fishery conflicts and perceptions of sea otters in California and Alaska. Sea Otter Conserv. 2015;2015:333–68. https://doi.org/10.1016/B978-0-12-801402-8.00012-3.

26. Wikle CK, Hooten MB. A general science-based framework for dynamical spatio-temporal models. Test. 2010;19:417–51. https://doi.org/10.1007/s11749-010-0209-z.

27. Williams PJ, Hooten MB, Womble JN, Esslinger GG, Bower MR, Hefley TJ. An integrated data model to estimate spatiotemporal occupancy, abundance, and colonization dynamics. Ecology. 2017;98(2):328–36. https://doi.org/10.1002/ecy.1643.

28. Bodkin JL, Udevitz MS. An aerial survey method to estimate sea otter abundance. In: Garner G, Amstrup S, Laake J, Manly B, McDonald L, Robertson D, editors. Marine Mammal Survey and Assessment Methods. Leiden: A. A. Balkema; 1999. p. 13–26.

29. Esslinger GG, Esler D, Howlin S, Starcevich LA. Monitoring population status of sea otters (*Enhydra lutris*) in Glacier Bay National Park and Preserve, Alaska–Options and Considerations. 201542. https://doi.org/10.3133/ofr20151119.

30. Esslinger GG. Sea Otter aerial survey data from Glacier Bay National Park and Preserve, 1999-2012: U.S. Geological Survey data release. 2019. https://doi.org/10.5066/P9SBAFF6.

31. Esslinger GG. Sea Otter aerial survey data from southeast Alaska, 2002-2003: U.S. Geological Survey data release. 2020. https://doi.org/10.5066/P9PYG92B.

32. Womble JN, Williams PJ, Johnson WF, Taylor-Thomas LF, Bower MR. Sea Otter Monitoring Protocol for Glacier Bay National Park, Alaska: Version SO-2017.1. Natural Resource Report NPS/SEAN/NRR–2018/1762. National Park Service, Fort Collins, Colorado; 2018.

33. Womble JN, Taylor LF. Glacier Bay sea otter count data from images (SO_D). Juneau: NPS SEAN; 2020. https://irma.nps.gov/DataStore/Reference/Profile/2.

34. Williams PJ, Hooten MB, Womble JN, Esslinger GG, Bower MR. Monitoring dynamic spatio-temporal ecological processes optimally. Ecology. 2018;99(3):524–35. https://doi.org/10.1002/ecy.2120.

35. Turchin P. Quantitative Analysis of Movement: Measuring and Modeling Population Redistribution in Animals and Plants. Sunderland: Sinauer Associates; 1998.

36. Hooten MB, Garlick MJ, Powell JA. Computationally efficient statistical differential equation modeling using homogenization. J Agric Biol Environ Stat. 2013;18(3):405–28. https://doi.org/10.1007/s13253-013-0147-9.

37. Williams PJ, Hooten MB, Womble JN, Bower MR. Estimating occupancy and abundance using aerial images with imperfect detection. Methods Ecol Evol. 2017;8(12):1679–89. https://doi.org/10.1111/2041-210X.12815.

38. Tinker MT, Yee JL, Laidre KL, Hatfield BB, Harris MD, Tomoleoni JA, Bell TW, Saarman E, Carswell LP, Miles AK. Habitat features predict carrying capacity of a recovering marine carnivore. J Wildl Manag. 2021;85(1): 303–23. https://doi.org/10.1002/jwmg.21985.

39. Bodkin JL, Esslinger GG, Monson DH. Foraging depths of sea otters and implications to coastal marine communities. Mar Mammal Sci. 2004;20(2): 305–21. https://doi.org/10.1111/j.1748-7692.2004.tb01159.x.

40. Johnson CK, Tinker MT, Estes JA, Conrad PA, Staedler M, Miller MA, Jessup DA, Mazet JAK. Prey choice and habitat use drive sea otter pathogen exposure in a resource-limited coastal system. Proc Natl Acad Sci U S A. 2009;106(7):2242–7. https://doi.org/10.1073/pnas.0806449106.

41. Gregr EJ, Nichol LM, Watson JC, Ford JKB, Ellis GM. Estimating carrying capacity for sea otters in British Columbia. J Wildl Manag. 2008;72(2): 382–8. https://doi.org/10.2193/2006-518.

42. Larson SD, Hoyt ZN, Eckert GL, Gill VA. Impacts of sea otter (*Enhydra lutris*) predation on commercially important sea cucumbers (*Parastichopus californicus*) in southeast Alaska. Can J Fish Aquat Sci. 2013;70(August):1498–507.

43. Estes JA. Natural history, ecology, and the conservation and management of sea otters. Sea Otter Conserv. 201519–41. https://doi.org/10.1016/B978-0-12-801402-8.00002-0.

44. Hoyt Z. Resource Competition, Space Use and Forage Ecology of Sea Otters in Southern Southeast Alaska. Phd, University of Alaska Fairbanks. 2015. https://doi.org/10.1017/CBO9781107415324.004.

45. Rumble J, Hebert K. Report to the board of fisheries, miscellaneous dive fisheries. Alaska Department of Fish and Game, Division of Commercial Fisheries, Fishery Management Report 11-59. Technical report. 2011. http://www.adfg.alaska.gov/FedAidPDFs/FMR14-46.pdf.

46. Shirley TC, Bishop G, O'Clair CE, Taggart SJ, Bodkin JL. Sea otter predation on dungeness crab in Glacier Bay, Alaska. In: High Latitude Crabs: Biology, Management and Economics. Fairbanks: Alaska Sea Grant College Program, University of Alaska; 1996. p. 96–02563576.

47. R Core Team, R Foundation for Statistical Computing. R: A language and environment for statistical computing. 2019. https://www.r-project.org/.

48. Garlick MJ, Powell JA, Hooten MB, McFarlane LR. Homogenization of large-scale movement models in ecology. Bull Math Biol. 2011;73(9): 2088–108. https://doi.org/10.1007/s11538-010-9612-6.

49. Okubo A. Diffusion and Ecological Problems: Mathematical Models. New York: Springer; 1980.

50. Cencini M, Lopez C, Vergni D. Reaction-diffusion systems: front propagation and spatial structures. Lect Notes Phys. 2003;636:187–210. https://doi.org/10.1007/978-3-540-39668-0_9.

51. Ebert U, Van Saarloos W. Front propagation into unstable states: Universal algebraic convergence towards uniformly translating pulled fronts. Phys D Nonlinear Phenom. 2000;146(1-4):1–99. https://doi.org/10.1016/S0167-2789(00)00068-3.

52. Conn PB, Johnson DS, Williams PJ, Melin SR, Hooten MB. A guide to Bayesian model checking for ecologists. Ecol Monogr. 2018;88(4):526–42. https://doi.org/10.1002/ecm.1314.

53. Kruschke J. Doing Bayesian Data Analysis: A Tutorial with R, JAGS, and Stan, 2nd ed. New York: Academic Press; 2015.

54. Gelman A, Carlin J. Beyond power calculations: Assessing type S (sign) and type M (magnitude) errors. Perspect Psychol Sci. 2014;9(6):641–51. https://doi.org/10.1177/1745691614551642.

55. U.S. Fish and Wildlife Service. NORTHERN SEA OTTER (Enhydra lutris kenyoni): Southeast Alaska Stock. Technical report. 2014.

56. Broms KM, Hooten MB, Johnson DS, Altwegg R, Conquest LL. Dynamic occupancy models for explicit colonization processes. Ecology. 2016;97(1):194–204. https://doi.org/10.1890/15-0416.1.

57. Weitzman BP. Effects of sea otter colonization on soft-sediment intertidal prey assemblages in Galcier Bay, Alaska. Master of arts, University of California Santa Cruz. 2013.

58. Estes JA, Jameson RJ, Rhode EB. Activity and prey election in the sea otter: Influence of population status on community structure. Am Nat. 1982;120(2):242–58.

59. Nicholson TE, Mayer KA, Staedler MM, Fujii JA, Murray MJ, Johnson AB, Tinker MT, Van Houtan KS. Gaps in kelp cover may threaten the recovery of California sea otters. Ecography. 2018;41(11):1751–62. https://doi.org/10.1111/ecog.03561.

60. Tinker MT, Doak DF, Estes JA. Using demography and movement behavior to predict range expansion of the Southern Sea Otter. Ecol Appl. 2008;18(7):1781–94. https://doi.org/10.1890/07-0735.1.

61. Hughes BB, Wasson K, Tim Tinker M, Williams SL, Carswell LP, Boyer KE, Beck MW, Eby R, Scoles R, Staedler M, Espinosa S, Hessing-Lewis M, Foster EU, Beheshti KM, Grimes TM, Becker BH, Needles L, Tomoleoni JA, Rudebusch J, Hines E, Silliman BR. Species recovery and recolonization of past habitats: Lessons for science and conservation from sea otters in estuaries. PeerJ. 2019;2019(12):1–30. https://doi.org/10.7717/peerj.8100.

62. Tinker MT, Hatfield BB, Harris MD, Ames JA. Dramatic increase in sea otter mortality from white sharks in California. Mar Mamm Sci. 2016;32(1): 309–26. https://doi.org/10.1111/mms.12261.

63. Lubina JA, Levin SA. The Spread of a Reinvading Species: Range Expansion in the California Sea Otter. Am Nat. 1988;131(4):526–43. https://doi.org/10.1086/284804.

64. Hooten MB, Lu X, Garlick MJ, Powell JA. Animal movement models with mechanistic selection functions. Spat Stat. 2020;37:100406. https://doi.org/10.1016/j.spasta.2019.100406.

65. Lewis JC, Chestnut T, Ransom JI, Werntz DO. Cascades fisher reintroduction project: Progress report for December 2015 to March 2017. Natural Resource Report NPS/PWR/NRR–2017/1486. 2017.

66. Estes JA. Growth and equilibrium in sea otter populations. J Anim Ecol. 1990;59(2):385–401. https://doi.org/10.2307/4870.

67. Riedman ML, Estes JA, Staedler MM, Giles AA, Carlson DR. Breeding patterns and reproductive success of California sea otters. J Wildl Manag. 1994;58(3):391. https://doi.org/10.2307/3809308.

68. Cole L. The population consequences of life history phenomena. Q Rev Biol. 1954;29(2):103–37.

69. Schmitz OJ, Lavigne DM. Intrinsic rate of increase, body size, and specific metabolic rate in marine mammals. Oecologia. 1984;62:305–9. https://doi.org/10.1007/BF00384261.

70. Bowen WD, McMillan J, Mohn R. Sustained exponential population growth of grey seals at Sable Island, Nova Scotia. ICES J Mar Sci. 2003;60(6):1265–74. https://doi.org/10.1016/S1054-3139(03)00147-4.

71. Louvrier J, Papaïx J, Duchamp C, Gimenez O. A mechanistic-statistical species distribution model to explain and forecast wolf (*Canis lupus*) colonization in South-Eastern France. Spat Stat. 2020;36:100428. https://doi.org/10.1016/j.wavemoti.2020.102529.

72. Wilmers CC, Estes JA, Edwards M, Laidre KL, Konar B. Do trophic cascades affect the storage and flux of atmospheric carbon? An analysis of sea otters and kelp forests. Front Ecol Environ. 2012;10(8):409–15. https://doi.org/10.1890/110176.

Publisher's Note